ChemComm

HIGHLIGHT

View Article Online
View Journal | View Issue

Cite this: *Chem. Commun.*, 2024, **60**, 7535

Catalyst development for O_2-assisted oxidative dehydrogenation of propane to propylene

Huimin Liu, *[a] Shaoyuan Sun,[a] Dezheng Li[a] and Yiming Lei *[b]

O_2-Assisted oxidative dehydrogenation of propane (O_2-ODHP) could convert abundant shale gas into propylene as an important chemical raw material, meaning O_2-ODHP has practical significance. Thermodynamically, high temperature is beneficial for O_2-ODHP; however, high reaction temperature always causes the overoxidation of propylene, leading to a decline in its selectivity. In this regard, it is crucial to achieve low temperatures while maintaining high efficiency and selectivity during O_2-ODHP. The use of catalytic technology provides more opportunities for achieving high-efficiency O_2-ODHP under mild conditions. Up to now, many kinds of catalytic systems have been elaborately designed, including transition metal oxide catalysts (such as vanadium-based catalysts, molybdenum-based catalysts, *etc.*), transition metal-based catalysts (such as Pt nanoclusters), rare earth metal oxide catalysts (especially CeO_2 related catalysts), and non-metallic catalysts (BN, other B-containing catalysts, and C-based catalysts). In this review, we have summarized the development progress of mainstream catalysts in O_2-ODHP, aiming at providing a clear picture to the catalysis community and advancing this research field further.

Received 24th April 2024,
Accepted 24th June 2024

DOI: 10.1039/d4cc01948b

rsc.li/chemcomm

1. Introduction

As one of the most important basic petrochemical raw materials, propylene can be used to produce various important organic chemicals, such as acrylonitrile, epichlorohydrin, epichlorohydrin, isopropanol, acetone, acrylic esters, *etc.*[1–4] With the outbreak of the shale gas revolution, the use of propane extracted from shale gas as raw material to prepare propylene can not only optimize the utilization of its low-carbon alkanes and by-products but also produce important basic organic chemical raw material, which has important practical significance.[5–7] Considering the fact that there are abundant shale gas resources in the world, it is expected that there will be sufficient shale gas production to cope with the significant supply–demand gap for propylene.[8]

[a] *School of Chemical and Environmental Engineering, Liaoning University of Technology, Jinzhou, 121001, Liaoning Province, P. R. China. E-mail: liuhuimin08@tsinghua.org.cn*
[b] *Departament de Química (Unitat de Química Inorgànica), Facultat de Ciències, Universitat Autònoma de Barcelona (UAB), Cerdanyola del Valles, 08193, Barcelona, Spain. E-mail: yiming.lei@uab.cat*

Huimin Liu

Huimin Liu is a professor at Liaoning University of Technology in the School of Chemical and Environmental Engineering. She received her PhD degree from Tsinghua University, China (2013), and then joined Kansai University (2013–2014), National Institute for Materials Science (2014–2017), and University of Sydney (2017) as a post-doctoral researcher. Her research interests are photochemistry, environmental chemistry, and heterogeneous catalyst design.

Yiming Lei

Yiming Lei received his MS degree from Tianjin University in 2022. In Jan. 2023, he joined Professor Liu's group as a Research Assistant at Liaoning University of Technology, China. Now, he is a PhD student in the Department of Chemistry at Universitat Autònoma de Barcelona, Spain. His current research focuses on the functionalization of the 2D germanene material for various practical applications such as (bio)sensor and photo/electrocatalysis, as well as the methane conversion and carbon dioxide reduction technologies.

The emergence of the catalytic energy conversion technique is one of the reliable strategies,[9–13] which can achieve the conversion of shale gas into propylene. Propane can undergo thermal cracking to release hydrogen and produce propylene under anaerobic conditions (direct dehydrogenation of propane), eqn (1).[14,15] With the assistance of suitable catalysts, at a reaction temperature of 590–630 °C, the one-way conversion rate of propane can reach 33–44%, and the selectivity of propylene is above 80%.[14,15] Although catalytic propane conversion is very promising and attractive from a thermodynamic view, the deep dehydrogenation of propane tends to form carbon deposition, which in turn leads to catalyst deactivation.[16,17]

Owing to the above problem, the O_2-assisted oxidative dehydrogenation process using propane as raw material and O_2 as a strong oxidant (oxidative dehydrogenation of propane (O_2-ODHP), eqn (2)) has attracted significant attention and has been considered as another effective process for producing propylene due to its remarkable cost advantage.[18–21] ODHP is a reversible and strongly endothermic reaction. Theoretically, the equilibrium constant of O_2-ODHP should increase with the increase of reaction temperature, but practically, its equilibrium constant still remains low at high temperatures. Therefore, from a thermodynamic perspective, O_2-ODHP needs to be carried out at high temperatures and low pressure. However, the high reaction temperature conditions intensify the over-oxidation of propylene, leading to a decrease in the selectivity of desired propylene. In this case, the fabrication of well-designed catalysts with tunable selectivity and high activity is important to directionally obtain the target product propylene from O_2-ODHP at low temperatures.

$$C_3H_8 \rightarrow C_3H_6 + H_2\ (+\text{Coke}) \quad (1)$$

$$C_3H_8 + 1/2O_2 \rightarrow C_3H_6 + H_2O \quad (2)$$

To date, a great number of catalysts have been developed for O_2-ODHP (Scheme 1), including transition metal oxide catalysts (such as vanadium-based catalysts, molybdenum-based catalysts, *etc.*), transition metal-based catalysts (such as Pt nanoclusters), rare earth metal oxide catalysts (especially CeO_2 related catalysts) and non-metallic catalysts (BN, other B-containing catalysts and C-based catalysts). Herein, the recent progress of these catalysts in O_2-ODHP is summarized and the underlying mechanism is revealed, with the aim to pave pathways for the rational design of more efficient catalysts for ODHP and advance this research field further.

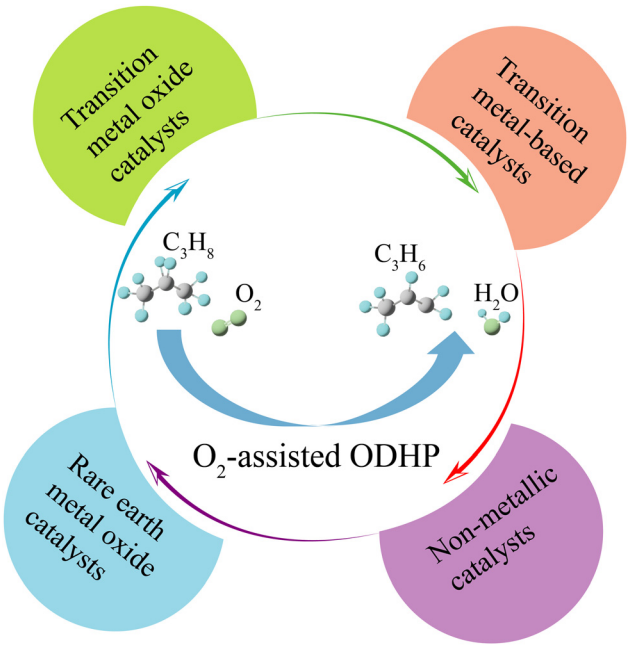

Scheme 1 Mainstream catalysts for O_2-ODHP.

2. Reaction mechanism in ODHP reaction

2.1. O_2-Assited ODHP reaction

O_2-ODHP attracts wide attention since it can induce chemical equilibrium by consuming H_2. Although the reaction routes might be different over diverse catalysts, some common features in the O_2-ODHP reaction mechanism could be summarized as follows: (i) interactions of C_3H_8 with the catalyst surface (weak/physical adsorption); (ii) dissociation of the C–H bond, leading to the formation of intermediate species; (iii) interaction of intermediates with adjacent surface oxygen and formation of C_3H_6; and (iv) cyclic reduction/reoxidation of the catalyst.[22] During the O_2-ODHP reaction, the coordination number of active centers will affect the ODHP process. For instance, high coordination number is beneficial for the insertion of oxygen species into C_3H_8 to generate partially oxygenated products or carbon oxides.[23] Meanwhile, the local environment of active centers can change between several configurations, suggesting that the catalytic O_2-ODHP might be related to the crystal structures of different types of catalysts.[24] The strength and reducibility of the oxygen ions also play an important role. What's more, the acid and/or basic centers on catalysts also affect the formation rate of olefinic intermediates and the desorption rate of products.

In the conventional ODHP reaction, the conversion of propane into C_3H_8 is endothermic and volume-increasing, meaning the conditions with high temperatures and low pressures are beneficial for achieving a high propane conversion rate. In practical industrial systems, the ODHP process is always conducted at 550–700 °C to achieve appreciable propylene yields.[25] However, the high temperature leads to side or competitive reactions, forming undesired C_2H_4 and CH_4 products due to C–C cracking. Meanwhile, coke is also one of the products from these side reactions. Therefore, it is necessary to consider the ability to dissociate C–H and avoid C–C bond break during the catalyst design steps.[26]

In order to selectively oxidize C_3H_8 to C_3H_6 and H_2/H_2O (eqn (1) and (2)), O_2 as an oxidant has several advantages including low reaction temperatures, resisting coke formation, and extending catalyst longevity.[27,28] The main challenge, as

mentioned above, is the overoxidation reactions, which oxidize C_3H_8 to CO and useless CO_2. In this review, the representative and recent works on catalyst design for ODHP using O_2 as the oxidant will be focused on, discussing the feasible strategies that can improve selectivity and stability under mild conditions.

Although some excellent reviews have summarized the catalytic systems for ODHP, they have focused on the relationship between ODHP performance and catalyst structures.[29–31] Other reviews have paid much attention to ODHP with CO_2 assistance[32] or the comparison of direct and CO_2-assisted ODHP (CO_2-ODHP).[26] Thus, the regulation of O_2-ODHP selectivity under mild conditions has not received enough attention. Considering the fact that ODHP technology could convert abundant shale gas into propylene, which is an important chemical raw material, and thus has practical significance, the representative works about utilizing catalyst design to improve the O_2-ODHP selectivity should be systematically reviewed to encourage more in-depth research in this area in the future.

2.2. CO_2-Assisted ODHP reaction

CO_2-ODHP ($C_3H_8 + CO_2 \rightarrow C_3H_6 + CO + H_2O$) is able to inhibit the formation of CO_2 by consuming H_2 *via* the reverse water–gas shift reaction (RWGS, $CO_2 + H_2 \rightarrow CO + H_2O$).[33] Besides the desired C_3H_6 and value-added syngas (CO and H_2) products, the coke from the dehydrogenation process can be removed *via* the reverse Boudouard reaction ($CO_2 + C \rightarrow 2CO$). Hence, it is possible to perform CO_2-assisted ODHP under high-temperature conditions with high efficiency and stability.

The mainstream mechanisms for CO_2-assisted ODHP are a direct route with a redox mechanism and an indirect route combining ODHP and RWGS reactions.[26] For the former, C_3H_8 interacts with O species to form C_3H_6 and water, and generates O vacancies over the catalyst surface. Then, CO_2 refills the O vacancies, supplying active O species and producing CO simultaneously. The direct route can be completed at a single active site or a dual site. Regarding the indirect route, ODHP and RWGS reactions could be completed to realize the simultaneous conversion of CO_2 and C_3H_8. During this pathway, the coke should be rapidly removed *via* the reverse Boudouard reaction.

Many research results about CO_2-ODHP have been published. For instance, Furukawa *et al.* reported a Pt–Co–In ternary nanoalloy on CeO_2 with $(Pt_{1-x}Co_x)_2In_3$ pseudo-binary alloy structure.[34] The synergistic effect of alloying platinum with indium and cobalt leads to high activity involving C_3H_6 selectivity and CO_2 reduction ability. The existence of Co species offers a high density of states near the Fermi level, reducing the energy barrier of CO_2 reduction. The cooperation between the alloy with CO_2 activation ability and CeO_2 with oxygen releasing ability facilitates coke combustion, thereby enhancing the catalyst stability. Song's group reported an efficient bifunctional CO_2-ODHP site capable of activating C–H and C=O bonds with inhibited C–C scission capacity.[35] In detail, their work proposed a La-modified binuclear Feoxo (La-Feoxo) site stabilized on a silicalite-1 support, achieving 32.7% C_3H_8 conversion with 83.2% C_3H_6 selectivity. The improvement should be attributed to the balance in the acid–base property due to FeO_x dispersion and La modification. The elaborate active site could stabilize HCOO* intermediates toward enhanced CO_2-assisted H removal efficiency.

At present, the main problem during CO_2-ODHP is the dry reforming of propane (DRP) competing reaction ($C_3H_8 + 3CO_2 \rightarrow 6CO + 4H_2$). The DRP reaction could be the dominant reaction under high-temperature conditions, converting too much C_3H_8 into CO instead of C_3H_6.[36] Therefore, to avoid the undesired DRP process, the C–H/C–C scission ability of C_3H_8 should be mainly focused on during the development of CO_2-ODHP catalysts.[37] A few works have summarized and discussed the soft oxidant-assisted ODHP system from three aspects: reaction mechanisms, catalyst composition, and oxidant footprint analysis. Interested readers are recommended to read ref. 29 and 34.

2.3. Chemical looping ODHP reaction

Although propane conversions are promising to get high-value-added chemicals, the traditional ODHP still has inevitable disadvantages, especially in the aspects of safety, high operation, and investment costs.[38] For example, when feeding C_3H_8 and O_2, the mixtures might evenly cause a potential explosion.[39] What's more, it is difficult to separate specific products from the product stream in traditional ODHP reactors, leading to high requirements for operation and equipment.[40] Although CO_2 as a soft oxidant has been developed to avoid oxidation, this weak oxidant also has its own limitations, such as high price as feedstock and downstream separation.[41,42]

In order to overcome the above disadvantages, chemical looping ODHP (CL-ODHP) combining dehydrogenation of propane and catalyst regeneration is explored and used in industries.[43] In a CL-ODHP system, the reaction routes include (i) the conversion of propane into propylene and water *via* active oxygen species (oxygen carrier) from lattice oxygen ($C_3H_8 + MO_x \rightarrow C_3H_6 + MO_{x-1} + H_2O$); (ii) transfer of the reduced oxygen carrier to the air reactor, where the missing lattice oxygen of the active phase is re-supplied by the air ($MO_{x-1} + 1/2O_2 \rightarrow MO_x$); and (iii) transfer of the re-oxidized oxygen carriers to ODHP reactors to complete the chemical loop. Therefore, through repeated reduction and oxidation of active species, the oxygen can migrate from the air reactor to the ODHP reactor and take part in the CL-ODHP process. The advantages of CL-ODHP include (i) the decline in energy consumption by H_2 oxidation; (ii) reduced investment and operation cost due to the elimination of separation equipment; (iii) avoidance of the potential explosion of C_3H_8; and (iv) reduced CO_2 emissions by indirect flameless combustion of H_2.[44,45]

The development of a suitable catalyst for CL-ODHP is crucial, but compared to the other two ODHP reaction systems, the investigations of catalyst design in the CL-ODHP field are much less. For instance, Gong's group designed

multifunctional ferric vanadate–vanadium oxide ($FeVO_4$–VO_x) redox catalysts by combining chemical looping-selective H_2 combustion and ODHP. VO_x provided dehydrogenation sites, and $FeVO_4$ acted as an oxygen carrier for H_2 combustion. After 200 chemical looping cycles for the re-oxidation of $FeVO_4$, $FeVO_4$–VO_x could maintain an integral performance of 81.3% propylene selectivity at 42.7% propane conversion. More importantly, the authors proposed a hydrogen spillover-mediated coupling mechanism. They believed that the H species generated at VO_x sites could transfer to adjacent $FeVO_4$ for combustion, leading to the formation of C_3H_6. The author's group also reported a MoO_3–Fe_2O_3 catalyst with a similar CL-ODHP mechanism.[46] Through introducing Mo species onto Fe_2O_3, the MoO_3–Fe_2O_3 catalyst achieved very stable catalytic behaviour after 300 cycles with ~49% propane conversion and ~90% propylene selectivity. Several works have comprehensively discussed the recent development of the CL-ODHP system,[39,47,48] and therefore the subsequent sections will mainly focus on O_2-assisted ODHP, which has not been systematically summarized in recent years.

3. Transition metal oxide catalysts

Transition metal oxide (TMO) catalysts, including vanadium-, molybdenum-, cobalt-, and nickel-based catalysts, mixed transition metal oxide catalysts, *etc.*, are excellent catalysts for O_2-ODHP because incompletely filled d-orbitals allow TMO to both donate and accept electrons easily from other molecules.[49] The real implementation of these catalysts in O_2-ODHP is reviewed in this sub-section.

3.1. Vanadium oxide-based catalysts

In the past several decades, vanadium-based catalysts have been the most extensively studied among transition metal oxide catalysts.[27,50] It has been reported that there are several strategies to improve the catalytic performance of vanadium-based catalysts in O_2-ODHP, mainly including (1) optimizing the distribution and amount of active site VO_x, (2) selecting a suitable catalyst support, and (3) introducing highly efficient promoters.

3.1.1. Optimizing the distribution and amount of active site VO_x. It is known that isolated tetrahedral vanadium oxide species containing terminal V–O groups (VO_x) are the active sites for the selective formation of propylene. The loading amount of active site VO_x directly affects the catalytic performance of vanadium-based catalysts in O_2-ODHP.[51,52] Actually, a relationship between the dispersion of VO_x and the selectivity of propylene has been observed and studied in several works. For instance, Puglisi *et al.* reported that, when the loading amount of VO_x exceeded 5.0%, the dispersion of active sites would decrease, which could easily lead to a decrease in catalytic activity (Fig. 1a).[52] Liu *et al.* found that when the loading amount of VO_x was low, the active site bridged oxygen

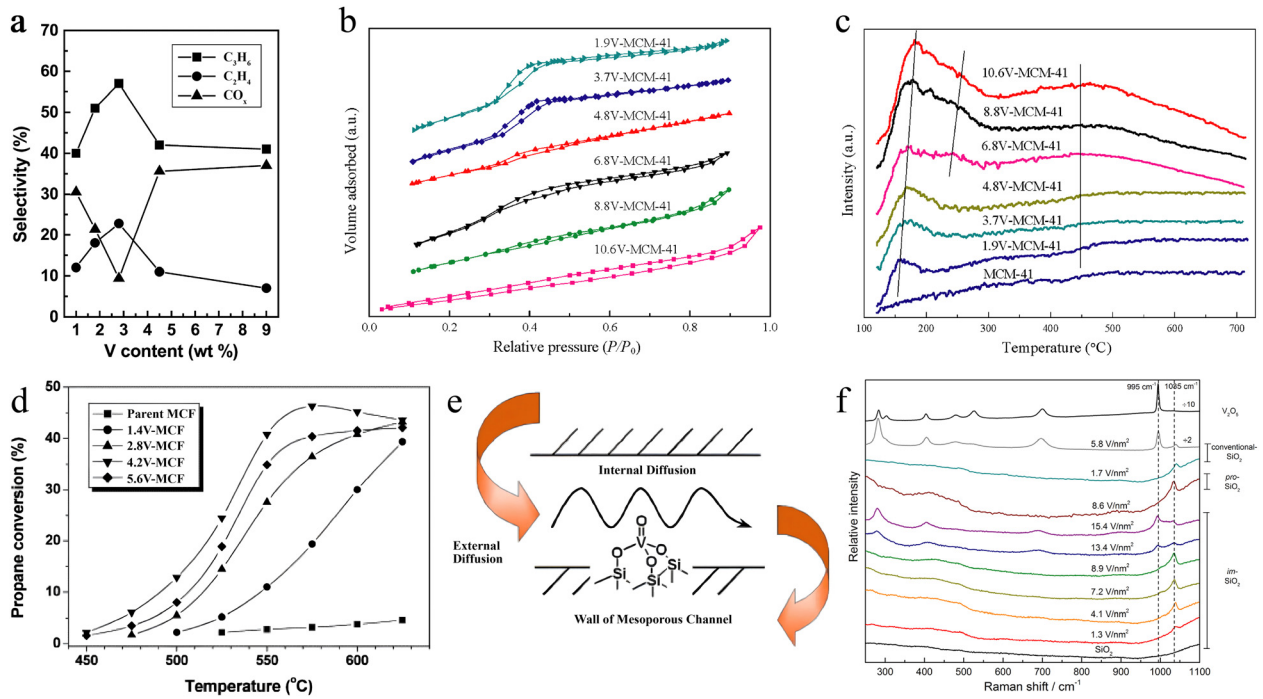

Fig. 1 (a) Variation of selectivity to propylene (■), ethylene (●), and CO_x (▲) with vanadium surface densities. Reaction temperature = 600 °C; propane conversion = 40%.[52] Copyright 2004 Elsevier. (b) N_2 adsorption–desorption isotherms of nV-MCM-41 samples. (c) NH_3-TPD profiles of nV-MCM-41 samples.[55] Copyright 2018 Elsevier B.V. (d) Propane conversion as a function of temperature on V-MCF catalysts. (Reaction conditions: C_3H_8 : O_2 : N_2 = 1 : 1 : 8; GHSV = 72 000 L kg_{cat}^{-1} h^{-1}.) (e) Schematic illustration of the molecular transport effect on V-containing mesoporous catalysts during the oxidative dehydrogenation of propane.[54] Copyright 2005 Elsevier. (f) Raman spectra of dehydrated vanadia catalysts supported on im-SiO_2, pro-SiO_2, and conventional-SiO_2, compared to the Raman spectra of im-SiO_2 (bottom) and bulk V_2O_5 (top).[58] Copyright 2015 American Chemical Society.

species, forming V–O–S (the oxygen species between the vanadium atom and the support) or V–O–V (the oxygen species between two vanadium atoms) species and thus realized good selectivity for propylene during catalytic O_2-ODHP.[53] Nonetheless, further increasing the loading amount of VO_x would result in agglomeration and generate V_2O_5 particles with low selectivity for propylene. The authors believed that the relationship between VO_x and selectivity should be attributed to the surface propyl species or adsorbed propylene over two V atoms of V–O–V species, benefiting the consecutive reactions and thus decreasing the selectivity to propylene from propane. Therefore, reasonable and proper regulation of the active site dispersion is crucial to improve the selectivity towards propylene.[53]

For regulating the dispersion of V active sites, Guo's group designed mesoporous nV-MCM-41 molecular sieves *via* surface engineering.[55] Compared to pristine V_2O_5, at low concentrations in nV-MCM-41, the V species existed in an amorphous state and became incorporated into the silicate framework or dispersed on mesoporous channels. The N_2 adsorption–desorption isotherms showed typical type-IV isotherms, suggesting the maintenance of the mesoporous structure after the addition of V species (Fig. 1b). The NH_3-TPD characterization was carried out to investigate the acidic characteristics. The results suggested that the isolated tetrahedral-like coordinated VO_x species had the properties of Lewis acid sites, which could be adjusted *via* changing the concentration of V elements (Fig. 1c). The optimal propane conversion rate could reach 58% accompanied by a propene selectivity of ~92% on 6.8 V-MCM-41. The authors believed that the improvement on catalytic efficiency and selectivity should be ascribed to the large specific surface of MCM-41 with a highly ordered mesoporous structure. But the increasing number of acidic sites reduced propene release from the V active sites, leading to deep oxidation and carbon deposition. This work also confirmed that suitably controlling the number and dispersion of VO_x sites on the substrate is a crucial factor for achieving efficient and selective O_2-ODHP reaction.

3.1.2. Selecting a suitable catalyst support. A catalyst support with specific structures, tunable absorption capacity, or special reactant activation sites generally endow the catalyst with unique properties, which then contribute to the catalytic performance.[56] Therefore, selecting a suitable support is an effective approach to improving the performance of vanadium-based catalysts in O_2-ODHP. Kung *et al.* demonstrated that the Lewis acidity of the support had a significant impact on the adsorption enthalpy of propane and propylene on the catalyst surface.[57] Higher Lewis acidity could cause strong interactions between propylene and the active metal (vanadium) centers. In this regard, a vanadium catalyst with low Lewis acidity was beneficial for the rapid desorption of propylene on the catalyst surface, which avoided overoxidation and consequently enhanced the selectivity towards the target product propylene.[57]

Another example of regulating activity and selectivity *via* utilizing the morphology and specific absorption sites on supports was reported by Fan *et al.*[54] Fan's group loaded vanadium on MCF at a loading amount of 4.2% and evaluated the catalytic performance in O_2-ODHP. Under the reaction temperature of 550 °C and atmospheric pressure conditions, the conversion of propane reached 40.8%, the selectivity of propylene was 68.5%, and the one-way yield was as high as 27.9% (Fig. 1d). The authors suggested that the larger specific surface area and the uniform pore size of the support MCF were beneficial for the rational dispersion of catalytic active sites (VO_x, Fig. 1e). Meanwhile, the weak acidity of MCF also promoted the selectivity of propylene.

Considering that the catalytic performance of supported VO_x is often influenced by its two- or three-dimensional dispersion, Grant *et al.* used an SiO_2 inert support (im-SiO_2) with low reactivity of surface SiOH groups toward the precursor to avoid undesired three-dimensional nanoparticles, which were often formed on conventional supports like Al_2O_3, TiO_2, Nb_2O_5, or ZrO_2.[58] Raman spectra suggested that im-SiO_2 did not show any sharp signal at 995 cm^{-1} from 3D V_2O_5, meaning the enhanced 2D dispersion behavior of V_2O_5 species (Fig. 1f). Because of the strong structure-sensitivity of O_2-ODHP, 2D V_2O_5 loaded im-SiO_2 had faster C_3H_8 consumption rate and higher TOF. Their results offered new opportunities for SiO_2-supported V-based oxides and even other metal oxides applied for O_2-ODHP.

3.1.3. Introducing highly efficient promoters. Adding suitable promoters into catalytic systems is an effective means to regulate the properties of the active site over the catalyst surface and thus improve the catalytic performance. For example, Grzybowska *et al.* added potassium (K) into the V_2O_5/TiO_2 system and adjusted the K/V ratio ranging from 0.01 to 0.20 for O_2-ODHP.[59] The propane conversion rate decreased considerably upon the addition of a small amount of K (K/V = 0.01), while the propane conversion rate changed slightly at higher K content (beginning from K/V = 0.05). Meanwhile, a distinct increase in the selectivity towards propylene was observed after the addition of a higher content of K (K/V = 0.05–0.10). Characterization suggested that the addition of K to the V_2O_5/TiO_2 catalyst led to a decrease in the acidity and an increase in the basicity of the catalytic system, which promoted the desorption of propylene on the catalyst surface and accordingly enhanced the ratio of propylene in the O_2-ODHP products.

Regarding the above vanadium-based catalysts, it is well accepted that their intrinsic activities originate from the strong redox properties of V^{5+} species. In O_2-ODHP, they follow the Mars–van-Krevelen mechanism, where oxygen is in zero order while propane is in first order.[60] However, in different catalytic systems, the types of active sites in vanadium-based catalysts might be varied, which include (1) bridged oxygen group (V═O); (2) bridged oxygen between vanadium and support (V–O–S); and (3) bridged oxygen between adjacent vanadium atoms (V–O–V). Therefore, making clear the type of active sites in a specific catalytic system and proposing novel reaction mechanisms are the remaining tasks for the future in-depth investigation of vanadium-based catalysts.

In addition to the above controversial active centers, the design of the VO_x-based catalyst also faces some challenges. In the O_2-ODHP area, extensive studies have been made on

VO_x-based catalysts.[61–63] It has been demonstrated that the catalytic behavior over VO_x is related to a series of parameters such as the oxidation state, coordination number, aggregation state, and reducibility of vanadium species. These parameters are not only affected by the loading amount of V but also by the properties of the carrier and the preparation of the catalyst.[64] Moreover, through the Mars–van-Krevelen mechanism, hydrocarbon molecules will react with oxygen species in VO_x to generate alkene and H_2O, and then reduced VO_x should be re-oxidized by gaseous oxygen molecules to regenerate the active VO_x sites. In this case, the whole process depends on the redox ability of VO_x-based catalysts, which is also important for VO_x catalyst design.

3.2 Molybdenum oxide-based catalysts

Similar to vanadium-based catalysts, molybdenum-based catalysts are also active in O_2-ODHP, but the activity of molybdenum-based catalysts is slightly inferior to their vanadium-based counterparts. It has been reported that the performance of molybdenum-based catalysts in O_2-ODHP is mainly affected by (1) the density of Mo on the catalyst surface; (2) the size of MoO_x species; and (3) the electronic structure of MoO_x species.

3.2.1. The density of Mo on the catalyst surface. Chen and co-authors studied the effects of Mo loading on the properties and performance of zirconia-supported molybdenum catalysts in O_2-ODHP.[60,65] The results revealed that the density of Mo on the catalyst surface and the pretreatment temperature of the catalysts strongly affected the structure of the molybdenum species. Polymolybdate domains were detected when the surface density of Mo was below 5 Mo nm^{-2}. At higher surface densities, Mo, MoO_3, and $ZrMo_2O_8$ were present, with their relative concentrations depending on the pretreatment temperature. The reaction rate of O_2-ODHP decreased with the increase of Mo surface density on the catalysts containing polymolybdate species and MoO_3, accompanied by an increase in the initial propylene selectivity. More in-depth discussion showed that high selectivity required complete coverage of the ZrO_2 surface by a mixture of molybdate oligomers. That is to say, the exposure of Zr–O–Mo chemical bonds was unfavorable for selective oxidation but contributed to the formation of CO_x *via* the combustion of C_3H_6.

3.2.2. The size of MoO_x species. Generally, the smaller the size of MoO_x species, which are the active sites for catalytic O_2-ODHP reaction, the more accessibility for them to contact the reactants propane and oxygen, leading to higher catalytic activity. For example, the above-mentioned Chen's work also revealed that the activities of $ZrMo_2O_8/ZrO_2$ decreased with the further increase of Mo surface density. It was owing to the increase of the particle size of active molybdenum species, which led to the lower accessibility of reactants to the catalytic active centers and thus the poorer activity.[65] Meanwhile, the authors also believed that the selectivity was related to the Mo=O bonds since weaker Mo=O bonds were involved in rate-determining C–H bond activation steps requiring lattice-given oxygen atoms. At similar Mo surface densities, the catalysts predominantly containing $ZrMo_2O_8/ZrO_2$ exhibited higher activities and lower initial propylene selectivity than those predominantly containing MoO_3 species.[65] This result indicated that the size of $ZrMo_2O_8$ domains increased with increasing Mo surface density without significant changes in the local structure or surface properties.

3.2.3. The electronic structure of MoO_x species. The electronic structure of MoO_x species could have an effect on its catalytic activity and selectivity towards the target products. Therefore, in recent years, more and more works have focused on the adjustment of electronic structures of Mo species. The effects of alkali oxides on the structure and catalytic behavior have been studied in the MoO_x/ZrO_2 catalyst during O_2-ODHP.[57] It demonstrated that two-dimensional polymolybdate domains were dominant active components with a surface density of Mo of 4 Mo nm^{-2} and alkali/Mo ratios of 0–0.2. The addition of alkali (Cs, K, Li) as a promoter did not change the structure of MoO_x domains; however, it influenced their electronic and catalytic properties. Propane conversion rates decreased monotonically with the increase of the alkali/Mo ratio and with the increase of the basicity of the alkali oxide (Cs > K > Li) (Fig. 2a). These alkali oxides strengthened Mo–O bonds in MoO_x domains and increased the reduction activation energies, which prohibited the initial reduction capability of MoO_x and finally slowed down the whole catalytic O_2-ODHP process (Fig. 2b). In contrast, the alkali oxides were of basic properties, which weakened the Lewis acidity of Mo^{6+} cations in MoO_x domains. The weaker Lewis acidity of Mo^{6+} promoted the rapid desorption of propylene on the active sites, leading to its higher selectivity. That is to say, alkali oxides as promoters could modify the electronic structure of MoO_x species, which accounted for the lower reaction rates and the higher selectivity towards propylene in O_2-ODHP.[66]

Gong *et al.* used two strategies including the coupling of surface acid catalysis and selective oxidation from lattice oxygen over MoO_3–Fe_2O_3, simultaneously, to promote propylene production.[46] They successfully introduced atomically dispersed Mo species on γ-Fe_2O_3 to create acid sites *via* the formation of MoO_3. The coupling strategies achieved a stable catalytic performance with 49% propane conversion and 90% propylene selectivity for more than 300 cycles. HR-XPS spectra showed the enrichment of Mo, which was beneficial for propane activation, and the increasing density of medium acid sites. NH_3-DRIFTS spectra suggested that the addition of Mo species caused both Lewis acid and Brønsted acid sites (Fig. 2c). The enrichment of Mo and modulation of acid properties accelerated the propane activation. Meanwhile, Mo also regulated the lattice oxygen activity, which led to selective oxidative dehydrogenation instead of over-oxidation in γ-Fe_2O_3 as confirmed by C_3H_8-D_2-TPSR results (Fig. 2d).

Similarly, Xie's group designed the coordination conditions of Mo atoms over single-crystalline Mo_2N and MoN monoliths for enhancing the non-oxidative dehydrogenation of propane to propylene.[67] Through simulation, the authors predicted the electron structures, suggesting that the high-density Lewis acid sites were from the top-layer Mo with electron deficiency

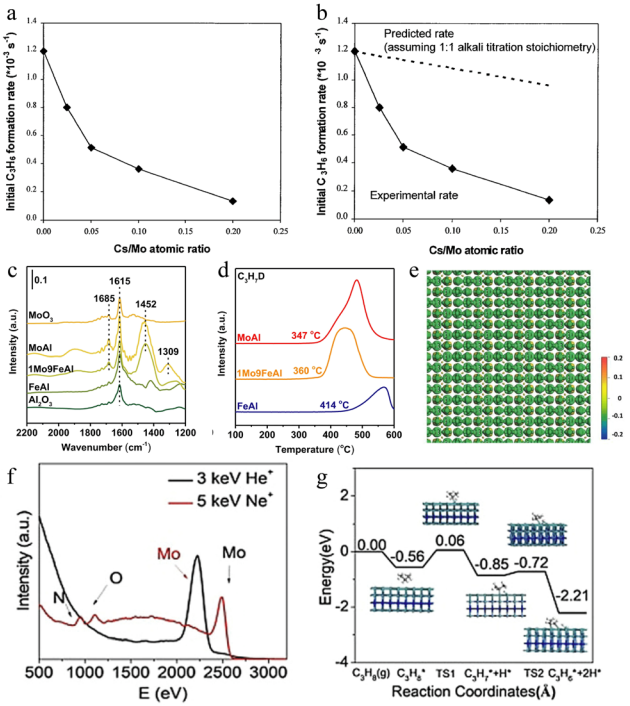

Fig. 2 (a) Dependence of the initial propylene formation rate on Cs–Mo/Zr catalysts with different Cs : Mo atomic ratio. (b) Comparison of dependence of the experimental and predicted initial propylene formation rate on Cs–Mo/Zr catalysts with different Cs : Mo atomic ratios. Reproduced with permission.[66] Copyright 2000 Elsevier. (c) NH_3-DRIFTS spectra of Al_2O_3, FeAl, 1Mo9FeAl, MoAl, and MoO_3. (d) Signal of C_3H_7D during C_3H_8-D_2-TPSR over FeAl, 1Mo9FeAl, and MoAl.[46] Copyright 2023 Springer. (e) Differential charge density diagrams of the (010) facet Mo_2N single crystal;[67] (f) HS-LEIS spectra of the top layer of the porous Mo_2N single crystal. (g) Potential energy profile for propane dehydrogenation on the Mo_2N (100) surface (C in gray, N in blue, Mo in green, and H in white). Copyright 2021 Wiley.

(Fig. 2e). Experimentally, HS-LEISS analysis further confirmed the atomic termination layer of Mo atoms for both Mo_2N and MoN. The electron-deficient status was favorable to receive electrons in C–H, accelerating the reactant dissociation and activation (Fig. 2f). The NH_3-TPD test clarified that the number of effective active sites (Lewis acid sites) on porous single crystals was higher compared to that on polycrystals. Taking Mo_2N as an example, the authors further calculated the energy barrier for each reaction step (Fig. 2g). The results showed that high-density acid sites achieved the low activation energy with a reasonable potential barrier. Therefore, the porous single-crystalline Mo_2N and MoN monoliths reached 11% propane conversion and ≈95–97% propylene selectivity under the mild conditions of 500 °C. The above works emphasized two facts: (i) catalysts containing exposed Mo active sites had excellent activity and tunable selectivity in O_2-ODHP and (ii) compared to blindly increasing the number of exposed sites, reasonably designing the effective active sites on the catalyst surface could improve the catalytic activity and selectivity considerably.

Despite extensive studies, the performance of molybdenum-based catalysts in O_2-ODHP is far from satisfactory, and even not comparable to their vanadium-based counterparts. In addition, molybdenum-based catalysts in O_2-ODHP are structure-sensitive. Sometimes, molybdenum-based catalysts obtained by similar preparation methods might exhibit different catalytic performances and even reaction pathways in O_2-ODHP.[68] All these disadvantages make it a challenging task to study molybdenum-based catalysts in O_2-ODHP.

3.3. Cobalt oxide-based catalysts

The variability of cobalt valence states enables it to function as a catalyst for O_2-ODHP. Cobalt oxide, cobalt-containing layered double-oxides (LDO), and cobalt-containing metal–organic frameworks have been investigated.

3.3.1. Cobalt oxide. The applicability of cobalt oxide in O_2-ODHP was discovered by Davies *et al.*, who studied the performance of Co_3O_4 nanocrystals in O_2-ODHP.[69] It was disclosed that at room temperature and ambient pressure, Co_3O_4 nanocrystals can convert propane into propylene, with propylene as the only product detected. However, Co_3O_4 nanocrystals suffered from low activity and severe deactivation. For improving selectivity, Song *et al.* designed ultrasmall cobalt oxide clusters encapsulated within silicalite-1 zeolites (CoO@S-1) *via* a ligand assisted *in situ* crystallization method.[70] The CoO@S-1 catalyst displayed enhanced activity with 13.66 $mmol_{propylene}\ g_{cat}^{-1}\ h^{-1}$ and a selectivity of >92% (Fig. 3a and b). The improved catalytic behavior should result from the encapsulated CoO clusters, which were favorable for propane adsorption and stabilizing the detached H* species from propane so that the dehydrogenation barriers were lower than those of framework Co^{2+} cations and Co_3O_4 nanoparticles (Fig. 3c). Besides, the π-binding propylene in CoO clusters could better avoid the over-dehydrogenation reaction than the di-σ binding propylene in metallic Co, thus leading to superior propylene selectivity and catalytic stability.

3.3.2. Cobalt containing LDO. The cobalt in LDO is highly dispersed, which might facilitate improvement of the performance of cobalt-based catalysts in O_2-ODHP. Huang and co-authors prepared a series of Co–Al LDO catalysts from pillared Co–Al layered-double-hydroxides, with different inorganic anions, including nitrate, carbonate, sulfate, and phosphate.[73] Compared with pure Co_3O_4, these Co–Al LDO catalysts possessed higher selectivity towards propylene even at a high propane conversion rate. Notably, Co–Al LDO catalysts with sulfate or phosphate anions exhibited better performance. Characterization results revealed that the Co–Al LDO catalysts consisted of uniformly dispersed Co_2AlO_x, containing both Co(III) and Co(II) species, with Co(III) being considered as the active center for O_2-ODHP. In addition, the incorporation of inorganic anions, especially sulfate or phosphate anions, also played an important role. For one thing, the anions reduced the particle size of the catalyst, and for another, they enabled the high dispersion of the active phase CoO_x, thereby improving the selectivity towards propylene.[73]

3.3.3. Cobalt-containing metal–organic frameworks. The cobalt species incorporated in metal–organic frameworks (MOFs) are also highly dispersed, which have also been shown

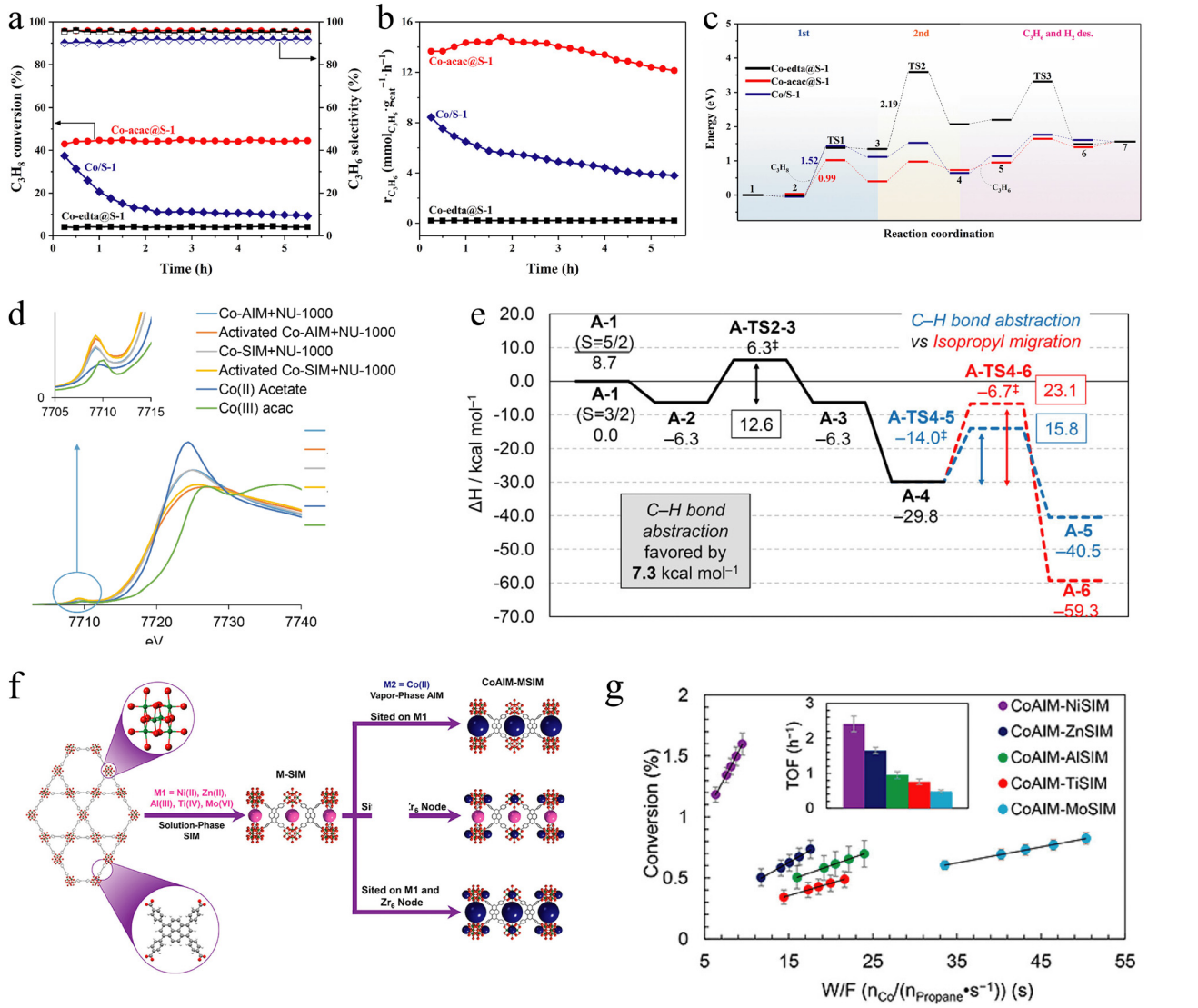

Fig. 3 (a) Propane conversion and propylene selectivity, 0.3 g catalyst, T = 600 °C, WHSV$_{C_3H_8}$ = 0.4 h^{-1}; (b) propylene formation rate tested under similar initial propane conversion; WHSV$_{C_3H_8}$ = 4.5, 3.125 and 0.4 h^{-1} for Co-acac@S-1, Co/S-1 and Co-edta@S-1; (c) the potential energy surface diagram.[70] Copyright 2006 Royal Society of Chemistry. (d) XANES spectra of Co-SIM and Co-AIM + NU-1000 before and after activation, along with the data for cobalt reference samples. (e) Reaction coordinate for propane ODH. ΔH_{503K} in kcal mol^{-1}.[71] Copyright 2016 American Chemical Society. (f) Schematic representation of the preparation of NU-1000-supported bimetallic catalysts. The promoter ions are anchored *via* SIM (pink) and Co ions are anchored *via* AIM (blue). (g) TOF values at 230 °C, as determined by varying the space velocity of propane.[72] Copyright 2017 American Chemical Society.

to be active for O_2-ODHP.[71,74] Farha *et al.* first applied cobalt-containing MOFs in O_2-ODHP. In this work, the NU-1000 MOF composed of $Zr_6(\mu_3\text{-}O)_4(\mu_3\text{-}OH)_4(H_2O)_4(OH)_4$ nodes and tetratopic 1,3,6,8-tetrakis(*p*-benzoate)pyrene (TBAPy4−) linkers was selected as a catalytic platform. They reported that these MOF-based catalysts afforded considerable propane activity and propylene selectivity below 230 °C and could maintain stable activity within 20 hours.[71] The Arrhenius plots for both the propane ODH and propene combustion processes were constructed. The *in situ* X-ray absorption results provided structural information on the deposited Co species. Both the Co-SIM+NU-1000 and Co-AIM+NU-1000 MOF samples had Co with +2 oxidation state (Fig. 3d). After 4 h activation, a slight increase in the intensity of the pre-edge peak and a decrease in the white-line intensity at ~7724 eV could be observed, indicating the formation of Co(III) species, which might be the active species for the O_2-ODHP reaction. The enthalpy reaction coordinate for O_2-ODHP was predicted, showing that owing to the competing transition states, the selectivity towards propene decreased with increasing reaction temperature (Fig. 3e). Further, theoretical calculations suggested that the active Co(II) ions were placed at the Zr_6 node of metal–organic frameworks, which had a lower activation energy barrier, thus exhibiting catalytic activity for propane under milder reaction conditions (Fig. 3f). They further modified the cobalt-based MOFs *via* a series of promoter ions with varying Lewis acidity involving Ni(II), Al(III), Ti(IV), and Mo(VI).[72] In O_2-ODHP, the activity of these catalysts increased in the order of

Mo(VI) < Ti(IV) < Al(III) < Zn(II) < Ni(II) (Fig. 3g), in accordance with the decreasing Lewis acidity of the promoter ion. The reason might be the decline of the Lewis acidity in the promoter ions, contributing to the formation of Co(III)-O species and the stabilization of a cobalt(III)oxyl/propane transition state.[72]

Cobalt-based catalysts exhibit high activities in O_2-ODHP application, but they still suffer from two main shortages. Firstly, the cobalt-based catalysts generally have strong oxidation ability. This property makes it easy for propane overoxidation, which ultimately leads to low selectivity towards propylene. What's more, due to the variability of cobalt valence states, the stability of cobalt-based catalysts during the O_2-ODHP process is poor, which remains an important concern.

3.4. Nickel oxide-based catalysts

Nickel oxide-based (NiO) catalysts have been widely studied in O_2-ODHP due to their low cost and comparable catalytic performance. The performance of NiO is generally poor, and several approaches have been developed to improve its performance, including (1) constructing mesoporous NiO; (2) doping NiO with foreign elements; and (3) loading NiO onto a suitable support.

3.4.1. Constructing porous NiO. Highly crystalline porous materials with oriented configurations are in demand for realizing high-performance energy conversion.[75] Without exception, compared to bulk NiO, mesoporous NiO possesses unique properties like abundant active sites and large surface area, which might contribute to its performance in O_2-ODHP. Experimentally, Li *et al.* discovered that, compared to NiO with an irregular pore structure, mesoporous NiO can achieve higher propylene selectivity and yield, recording a propane conversion of 25.8% and a propylene yield of 13.2% at 450 °C, as well as good stability within 72 hours.[76] Characterization analysis suggested that mesoporous NiO possessed more O^- species and cation vacancies (Fig. 4a), resulting in a significant difference in their catalytic performance. In addition, due to the presence of mesopores, the diffusion and transfer of reactant and product molecules were easier on mesoporous NiO, which also played an important role in improving its performance.[76] Although the mesoporous NiO catalysts are promising for improving the propylene evolution rate, the actual synthesis of a 3D-oriented mesostructure configuration is extremely more difficult than imaging it.[77] Many irregular mesoporous materials have amorphous or polycrystalline pore walls, adversely decreasing the transport and migration of electrons, ions, and guest molecular species.[78] Thus, it is necessary to design and fabricate mesoporous NiO catalysts reasonably, which is one of the main challenges in the material structure engineering field.

Liu's group fabricated ordered mesoporous Ni–Mo–O catalysts *via* a two-step method involving a hard template and impregnation steps.[79] The results of pore size distribution displayed the ordered mesoporous characteristic of Ni–Mo–O catalysts with a low ratio of Mo/Ni (Fig. 4b). Similarly, SEM images revealed a mesoporous structure when the concentration of Mo was low (Fig. 4c). TEM images suggested that the elimination of the mesoporous structure with the higher concentration of Mo should be attributed to the blockage of mesoporous channels due to the impregnation of Mo species (Fig. 4d). H_2-TPR characterization showed that the addition of Mo could inhibit the reducibility of the Ni species according to the shift of the characteristic peaks toward the high temperature side (Fig. 4e). With an excellent mesoporous morphology and suitable redox ability, the Ni–Mo–O catalyst with a Mo/Ni ratio of 0.4 shows the highest activity with a propylene yield of 15.6%. The authors believed that the Ni–Mo–O catalyst was favorable for the C–C bond cleavage, which was the reason for the high selectivity of propylene. On the other hand, the decreased reducibility also contributed to the high selectivity because pure NiO with high redox ability and a lot of chemisorbed oxygen species would have strong reaction activity during the first step of OHDP.

3.4.2. Doping NiO with foreign elements. Doping a foreign element into NiO is one of the strategies to regulate the physicochemical properties and catalytic performance of NiO. Up to now, many dopants, such as Ti,[80] Zr,[83] Ta,[84] and Ce,[85] have been reported in NiO-based O_2-ODHP systems. Here we take Ti-doped NiO as an example for illustration. Wu *et al.* prepared a Ni–Ti–O catalyst by a sol–gel method and reported that compared with NiO, Ni–Ti–O exhibited higher selectivity towards propylene, affording a propane conversion of 28.4%, a propylene selectivity of 42.5%, and a propylene yield of 12.1% at 300 °C (Fig. 4f).[80] There was a strong interaction between NiO and TiO_2, due to the differences in lattice parameters and valence states of Ni^{2+} and Ti^{4+}. The strong interaction weakened the reduction ability of the catalyst, which led to a decrease in activity and an increase in selectivity towards propylene in O_2-ODHP.[80]

Besides, multielement-doped NiO catalysts were also developed for O_2-ODHP. For instance, Ce_3NbNiO catalysts have been prepared by a sol–gel method.[81] Compared to pristine NiO, Ce_3NbNiO presents a higher propane conversion with higher propene selectivity at a relatively low temperature (250 °C). The enhancement effects of both Ce and Nb were investigated. O_2-TPD measurements confirmed that Ce-doping increased the number of electrophilic oxygen species (Fig. 4g), which were mostly responsible for the deep oxidation reactions, so the propane conversion rate was largely improved. For the role of the Nb element, NH_3-TPD proved the formation of weak acid sites (Fig. 4h). Since the higher strength and more acid sites over the catalyst surface could decrease the selectivity to olefin. The weak acid sites induced by Nb-doping should contribute to a decline in surface acidity and further improve the propene selectivity of the Ce_3NbNiO catalyst.

Besides doping Ni-based catalysts, introducing Ni into other oxide catalysts is another elemental doping idea to improve the activity and selectivity. For instance, Ni doped CeO_2 nanorod catalysts for O_2-ODHP have been reported.[86] Based on the periodic DFT calculations, the authors proposed a potential strategy to improve catalyst performance towards O_2-ODHP. In detail, surface hydroxylation enhanced the propylene selectivity *via* inhibiting the formation of oxygenates and the formation of

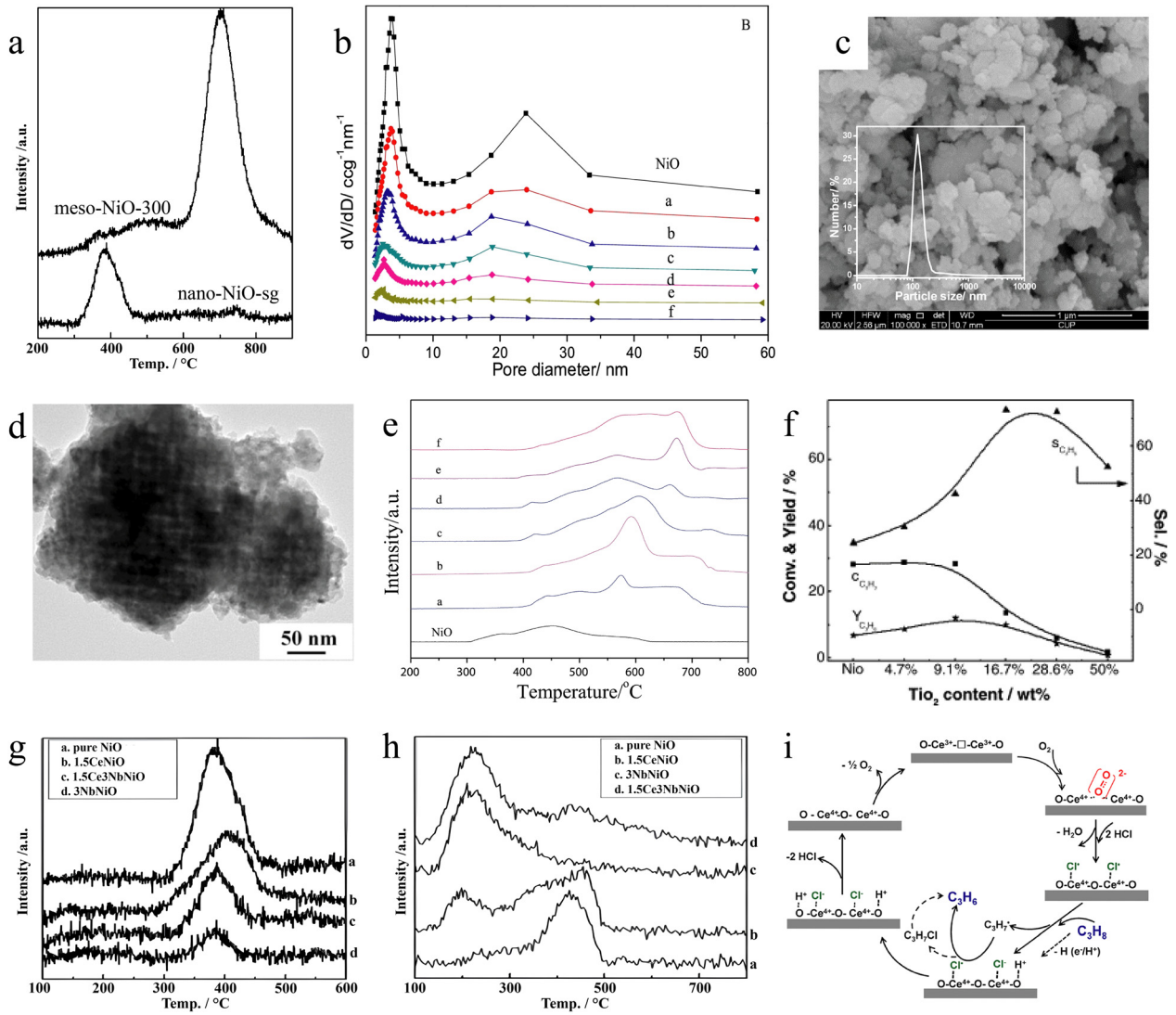

Fig. 4 (a) O_2-TPD spectra of nano-NiO-sg and meso-NiO-300 samples.[76] Copyright 2010 Elsevier. (b) Pore size distribution of mesoporous NiO support and Ni–Mo–O catalysts [(a) Mo/Ni = 0.05, (b) Mo/Ni = 0.1, (c) Mo/Ni = 0.2, (d) Mo/Ni = 0.3, (e) Mo/Ni = 0.4, (f) Mo/Ni = 0.5]. (c) SEM images and particle size distribution (inset) of mesoporous Ni–Mo–O catalysts: Mo/Ni = 0.05. (d) TEM images of mesoporous Ni–Mo–O catalysts: Mo/Ni = 0.5. (e) H_2-TPR profiles of mesoporous NiO and Ni-Mo-O catalysts [(a) Mo/Ni = 0.05, (b) Mo/Ni = 0.1, (c) Mo/Ni = 0.2, (d) Mo/Ni = 0.3, (e) Mo/Ni = 0.4, (f) Mo/Ni = 0.5].[79] Copyright 2019 Elsevier B.V. (f) Catalytic data obtained at 300 °C for Ti–Ni–O catalysts as a function of TiO_2 content.[80] Copyright 2005 Elsevier. (g) O_2-TPD spectra of pure and Ce/Nb-doped NiO catalysts (200 mg sample). (h) NH_3-TPD spectra of pure and Ce/Nb-doped NiO catalysts (200 mg sample).[81] Copyright 2010 Springer. (i) Proposed reaction mechanism for the oxidative dehydrogenation of C_3H_8 to C_3H_6 by O_2 in the presence of HCl over CeO_2-based catalysts.[82] Copyright 2018 American Chemical Society.

acetone. Compared to surface oxygen species, hydroxyls were more beneficial for the H abstractors, leading to an elementary mechanistic transformation in propene formation from MvK to LHHW. Thus, the Ni doping and surface hydroxylation (Lewis base addition) could be a reliable strategy for achieving selective O_2-ODHP. Another example of Ni as a foreign doping element was reported by Farin *et al.*[87] This work fabricated mesoporous β-$NiMoO_4$ using Ni as the guest ion. Due to the coordination by the copolymer COO^- functions, Ni cations were stable in the main β-phase. The presence of Ni species and the large specific surface from the mesoporous structure maintained a high activity level (propane conversion = 14.1%) and also reached high propylene selectivity (propene selectivity = 72%).

3.4.3. Loading NiO onto a suitable support. Loading NiO onto suitable support is a means to improve its dispersion and further enhance its catalytic O_2-ODHP activity.[76,88] Moriceau *et al.* loaded NiO onto CeO_2 and prepared the NiO/CeO_2 catalyst through co-precipitation and impregnation methods.[89] 1NiO/CeO_2 achieved a propane conversion of 12.0% and a propylene selectivity of 60.0% at 300 °C, which were superior to those of pure NiO and CeO_2. The highly dispersed NiO_x species were the active species for O_2-ODHP. When the loading amount of NiO was low, the CeO_2 surface was gradually covered with the

dispersed NiO_x species with higher surface potential values than that of CeO_2. Because NiO_x was considered to be an active center in O_2-ODHP, the high dispersion of NiO_x on the support surface could lead to higher propylene selectivity. However, as the loading amount of NiO increased, the selectivity towards propylene decreased, because crystallized NiO formed, which was unfavorable for propylene production.[89]

Another work about the NiO/CeO_2 catalyst was recently reported by Wang's group.[82] The authors investigated the relationship between catalytic behavior and exposed facets of CeO_2 nanocrystals. The results showed that the [1 1 0] and [1 0 0] facets on the nanorod had the highest activity, and the nanocube enclosed by [1 0 0] facets possessed the most selectivity for propylene evolution. More importantly, the NiO modification achieved a single-pass propylene yield of 55% and outstanding stability with more than 100 h activity. The DFT and mechanistic studies suggested that the determining factors for enhanced activity and selectivity should be the surface oxygen vacancy and the surface chloride coverage (Fig. 4i). In detail, the peroxide species (O_2^{2-}), which was formed by adsorption of O_2 on surface oxygen vacancies, activated chloride and led to a radical-like active chlorine species. Further, the active chlorine species induced the dissociation of the C–H bond in propane, forming propylene as a major product.

3.5. Mixed transition metal oxide catalysts

In addition to the monometallic catalysts, some mixed TMO catalysts have also been studied in O_2-ODHP, such as V–Mo mixed oxide,[90] Nb–V mixed oxide,[91] Mo–V–Te–Nb mixed oxide,[92] and so on. Take the application of V–Mo mixed oxide in O_2-ODHP as an example. Alasiri *et al.* prepared a series of V–Mo mixed oxide catalysts with varied Mo/V ratios (Mo/V = 1/1, 7/3, 8/2, and 9/1) using a modified citrate–nitrate auto-combustion method and applied the catalysts for O_2-ODHP.[90] In the Raman spectra of V–Mo mixed oxides (Fig. 5a), a peak at 785 cm^{-1} assigned to the vibration of V–O–Mo in a polymolybdovanadate species indicated that in all of the V–Mo mixed oxide catalysts, there was an interaction between the molybdenum and vanadium metal ions, which was effective for O_2-ODHP. In ODHP, the catalyst with a Mo/V ratio of 9 : 1 gave the highest yield and selectivity of propylene, reaching a propylene yield of 4.8% and a propylene selectivity of ~100.0% at 500 °C.

Recently, Hess *et al.* designed a VO_x/TiO_2 catalyst.[93] Compared to conventional P25, which always caused carbon deposition during the O_2-ODHP process, the active sites was located at VO_x instead of TiO_2. And UV-Raman spectroscopy showed that vanadia-related features at 858, 936, 991, and 1024 cm^{-1} were attributed to interface V–O–Ti, bridging V–O–V, the terminal vanadyl bond of V_2O_5, and the terminal vanadyl bond of amorphous vanadia, respectively (Fig. 5b). The O_2-ODHP reaction involved preferentially the V=O bonds of dimeric species instead of doubly bridged V–O–V bonds. With a high density of V active sites, the oligomeric V with better reducibility avoided the undesired oxidation process. The *operando*/transient spectroscopic results clarified that TiO_2 could transfer H species from propane to V active sites based on Ti–OH groups on anatase (Fig. 5c). Therefore, the determining step of the C–H bond dissociation could be accelerated, improving the whole O_2-ODHP efficiency.

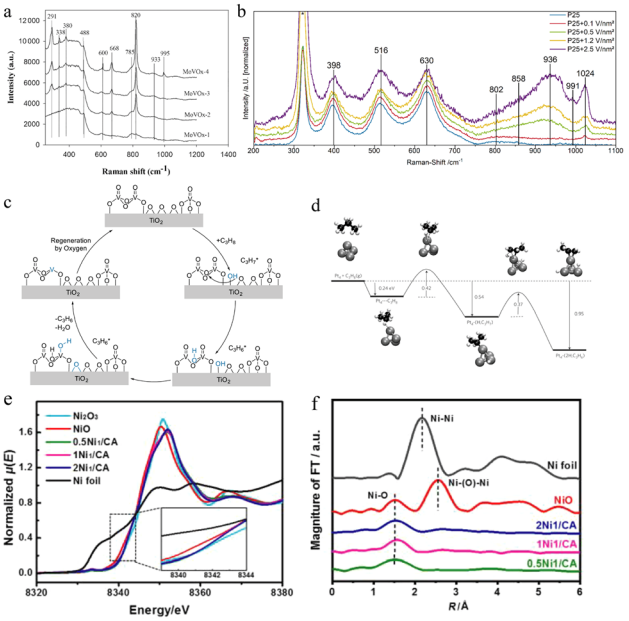

Fig. 5 (a) Raman spectroscopy of $MoVO_x$-1–4.[90] Copyright 2019 Wiley. (b) Normalized UV-Raman spectra (385 nm) of bare P25 and vanadia-loaded samples. The signal from the used CaF_2 window is marked with an asterisk. (c) Proposed reaction mechanism for the ODH of propane over vanadia-loaded titania (P25) based on *operando* and transient spectroscopic analyses.[93] Copyright 2023, American Chemical Society. (d) Diagram of primary reaction steps.[19] Copyright 2009 Springer. (e) Ni K-edge XANES spectra and (f) Ni K-edge FT-EXAFS spectra of Ni1/CA catalysts and reference samples.[107] Copyright 2023 Wiley.

As a typical p-type semiconductor, NiO can adsorb various types of oxygen species on its surface even under mild conditions.[94] Thus, it has been confirmed that NiO is able to realize O_2-ODHP at low temperatures, suggesting its great potential for the practical industry.[95,96] However, there are still some challenges in NiO-based catalytic systems. NiO with poor stability is easily reduced to Ni^0, and single NiO is hard to use as a stable catalyst with high catalytic performance.[97] Although some NiO-based composite oxides, such as Ni–Ce–O, Ni–Nb–O, and Ni–Ti–O, have been developed for improving stability during the O_2-ODHP process, the propylene yield rates are still very low.[80,89,98] Therefore, how to simultaneously improve stability and reaction efficiency is an urgent problem when designing NiO-based catalysts. Recently, it has been reported that polyoxometalates possess the ability to activate molecular oxygen at moderate temperatures, so this new family has been developed for selective oxidation of light alkanes.[99,100] Introducing polyoxometalates into NiO-based catalysts might be a reliable strategy to overcome the current problems.

4. Transition metal-based catalysts

Transition metal-based catalysts are generally applied in the direct dehydrogenation of propane. Hence, their studies in

O_2-ODHP are quite limited. The most common transition metal-based catalysts in O_2-ODHP are Pt-based catalysts. Pt-based catalysts have been used for the total combustion of propane, which is the prevailing reaction at temperatures lower than 500 °C.[101] In 2009, Vajda *et al.* reported that the subnanometer Pt cluster as the active phase exhibited excellent performance in O_2-ODHP.[19] Pt_{8-10} atomic clusters gave a propane conversion rate of 21.9% and a selectivity towards propylene of 64.0% at 500 °C, with the turnover frequency far superior to that of the classic VO_x/Al_2O_3. Theoretical DFT calculations suggested that on the Pt clusters, compared to other C–H and C–C bonds, the C–H bond on the methylene group of propane was more likely to break first, forming propyl radicals, which then extract the protons from the methyl group to generate propylene (Fig. 5b). The excellent catalytic performance of Pt clusters might be attributed to the sub-nanometer level Pt_{8-10} active phase and its high dispersion. The main problem in Pt-based catalytic systems is agglomeration and sintering. To deal with this problem, Furukawa's group designed a Pt–Co–In ternary nanoalloy on a CeO_2 support. The strong activation ability in the $(Pt_{1-x}Co_x)_2In_3$ pseudo-binary alloy and the oxygen releasing ability in CeO_2 facilitated Mars–van Krevelen-type coke combustion, thus improving the catalyst stability.[34] In addition to transition metal-based catalysts containing noble metals, Yao *et al.* reported a cheap Ni-based catalyst ($Ni@BO_x$/BN).[102] With the assistance of the Ni subsurface, the *in situ* growth of BO_x significantly increased the catalytic activity. The authors believed that the enhancement of catalytic efficiency should be attributed to the strong affinity of the Ni subsurface, which reduced the energy barrier for producing active species. In this case, the balance between B–OH cleavage and regeneration of boron hydroxyl groups could be achieved under low-temperature conditions.

Besides the above metallic and alloyed transition metal-based catalysts, single-atom catalysts (SACs) are one of the most recent, revolutionary, and rapidly developing research fields in catalytic science.[103] SACs inherit the advantages of easy separation and good recyclability of supported metal nanostructured catalysts and also combine the characteristics of homogeneous catalysts with highly homogeneous active centers and an adjustable coordination environment.[104] The coordination between single atoms and the support involves strong interaction or charge transfer, conferring unique electronic and geometrical structures to individual metal atoms, differing from that of conventional metal NPs and carrying some charge.[105] The high activity of valence electrons, the quantum confinement effect, and the sparse quantum level of metal atoms contribute to the maximum surface free energy of the metal species in SACs, which facilitates chemical interactions between single atoms and the support.[105] In the O_2-ODHP field, some SAC catalysts were also designed and fabricated. For example, Liu's group achieved the loading of PtSn-SA over commercial nano-Al_2O_3 with 0.1 wt% Pt.[106] By combining *in situ* characterization and theoretical calculations, the Sn_1Pt single-atom alloy structure could be confirmed, showing high efficiency with 47.6 mol g_{Pt}^{-1} h^{-1} of C_3H_6 evolution rate and more than 40 h of long-term stability. The results of *in situ* diffuse reflectance infrared Fourier-transform spectroscopy (DRIFT) suggested that the coke deposition could be inhibited *via* Sn_1Pt single-atom alloy mediated reconstruction, contributing to stability enhancement. Besides the noble-metal SACs, Zhang *et al.* reduced the size of transition metals and synthesized a Ni-based single-atom catalyst for O_2-ODHP.[107] X-ray absorption spectroscopy (XAS) confirmed the oxidation state (Ni^{3+}) of Ni species on the CA support (Fig. 5c). EXAFS showed the isolated features of the metal Ni species, meaning the successful construction of the Ni-based SAC catalyst (Fig. 5d). Ni-SA supported on calcium aluminate was highly effective in O_2-ODHP (Fig. 5e and f), recording a propylene selectivity of 47.3%, a yield of propylene of 14.2%, and good stability for 20 hours of testing, which was 2–3 times better than that of Ni nanoparticles. XPS characterization elucidated the reason for the improved efficiency and selectivity. The more positive electronic properties of the Ni-SA sites were beneficial for the activation of oxygen molecules (propylene desorption), effectively inhibiting further oxidation of propylene to CO_x by-products.

Although the above works proved that transition metal-based catalysts are efficient for O_2-ODHP, the synthesis process of the clusters and single-atom catalysts is quite complex, requiring accurate and strict control, which limits the industrial application of clusters and single-atom catalysts in O_2-ODHP. Meanwhile, in some transition metal-based catalysts containing noble metals, their high cost is also another disadvantageous factor, limiting their large-scale applications and leading to higher requirements in their activity, stability, and recyclability.

5. Rare earth metal oxide catalysts

Among the rare earth metal oxide catalysts for O_2-ODHP, CeO_2-based catalysts are mainly focused on because of their excellent oxygen storage and release properties,[108,109] and strong redox properties.[82,110]

The performance of pure CeO_2 is still not ideal for industrialization, evidenced by the high propane conversion rate but extremely low propylene selectivity, owing to the occurrence of overoxidation. Modifying CeO_2 by NiO,[82] Cl,[110] F,[111] or P[112] could improve its performance. For instance, Wan *et al.* demonstrated that F-modified CeO_2 could selectively promote the production of propylene.[111] After further modification by an appropriate amount of Cs, the catalyst with the composition 3% Cs_2O/CeO_2–$2CeF_3$ achieved a propylene yield of more than 30.0% at 500 °C. CeF_3 played two functions in 3% Cs_2O/CeO_2–$2CeF_3$ for O_2-ODHP: one is that the surface F replaced some lattice oxygen in CeO_2, promoting the migration of oxygen species and the activation of surface oxygen species; and another is that the addition of F resulted in a highly dispersed surface CeO_2 active phase. The modification of CeO_2 by P could also facilitate the dispersion of the surface active phase CeO_2, thus improving propylene selectivity.[112] As a result, at the

reaction temperature of 550 °C, $CePO_4$ recorded a propylene selectivity of 62.0%, much higher than that of CeO_2 (31.0% under the same reaction conditions).

Although there are some studies on the application of rare earth CeO_2-based catalysts in O_2-ODHP, the enhancement effect from the rare earth metal oxides has not been extensively investigated and utilized in the O_2-ODHP area. The reaction mechanism is not clear yet. Thus, more efforts should be devoted to this kind of catalytic system to elucidate the possible theories.

6. Non-metallic catalysts

Non-metallic catalysts, such as boron nitride (BN), other B-containing catalysts, and C-based catalysts, have also been developed for O_2-ODHP. In this sub-section, we will review the current progress of these catalysts in O_2-ODHP.

6.1. BN catalysts in O_2-ODHP

Among the non-metallic catalysts, the performance of BN is relatively excellent,[113] Since there have been some reviews on the development of BN catalysts,[114–117] the progress of BN in only O_2-ODHP is briefly summarized here.

The application of BN in O_2-ODHP was initiated in 2016 when the Hermans group reported that commercial hexagonal BN and BN nanotubes exhibited much higher catalytic activity and propylene selectivity in O_2-ODHP than other catalysts.[118] For example, on a commercial hexagonal BN catalyst, at a reaction temperature of 490 °C, the conversion of propane was 14.0%, the selectivity of propylene could reach 79.0%, and there was almost no complete oxidation product CO_2 generated. In addition, BN also exhibited very high stability in O_2-ODHP. The rich hydroxyl groups at the edge endowed BN with an initial propane conversion rate of 20.6% and an initial propylene selectivity of 80.2% at a reaction temperature of 530 °C in O_2-ODHP.[119] Besides, its activity and selectivity remained almost unchanged within 300 hours. The excellent catalytic performance of BN has opened up a new path for the selective cleavage of C–H bonds in alkanes and has become a research hotspot. From then on, several approaches have been adopted to improve the performance of BN in O_2-ODHP, which include (1) increasing the specific surface area of BN;[120] (2) doping BN with foreign elements;[121] (3) preparing BN with a local chemical environment regulated by plasma, and so on.[122] Here some typical examples are illustrated.

6.1.1. Increasing the specific surface area of BN. Increasing the specific surface area of BN can increase the exposure probability of B and the number of active site BO_x generated by BN in an oxygen-containing atmosphere, which is one of the effective means to improve its performance in O_2-ODHP. For example, Chaturbidy *et al.* reported that high specific surface area can improve the performance of hexagonal BN in O_2-ODHP.[120] The N_2 adsorption–desorption measurements showed the type IV isotherm with a Brunauer–Emmett–Teller (BET) specific surface area (SSA) of 1380 $m^2\ g^{-1}$. At a reaction temperature of 525 °C, the catalyst exhibited a high propane conversion rate (~50.0%), high olefin selectivity (total selectivity of propylene and ethylene is about 70.0%), and good stability of 100 hours by co-feeding with ammonia. Owing to the large surface area, there was no coke deposition, which could deactivate the BN catalyst, beyond 5 h proved by thermogravimetric analysis (TGA) measurements.

6.1.2. Doping BN with foreign elements. Doping BN with foreign elements could tailor its physicochemical properties and introduce new functional groups into BN, which might have an effect on the performance of doped BN in O_2-ODHP. For example, it has been revealed that doping a small amount of C into BN could enhance the incorporation of O atoms into the BN lattice, leading to the generation of more active species for O_2-ODHP.[124] However, if an excessive amount of C was doped into BN, the catalyst would suffer from decomposition and sintering severely, which consequently could result in a decrease in catalytic activity. Therefore, the valence of foreign elements doped into BN should be well regulated. Over the BN catalyst with an optimized amount of C doping, a propane conversion of 18.5% and a propylene selectivity of 82.3% were realized at 500 °C. FTIR and XPS spectra clarified the oxygen functionalization on the BN-M surface (Fig. 6a and b). After catalytic O_2-ODHP reactions, the surface nitrogen dropped sharply to 18.8%, while the total oxygen increased to 29.3%. This phenomenon confirmed the formation of BO_x active sites, leading to the replacement of N by O over the catalyst surface. However, high oxygen content and a large amount of BO_x species implied the overoxidation of the catalyst, resulting in poor catalytic stability, which was proved by other BN-based catalysts with a total oxygen content of 37.3%. Therefore, the authors believed that the appropriate ratio of BN and BO_x was the key to ensure the high activity and stability of the catalyst.

6.1.3. Preparing BN with a local chemical environment regulated by plasma. The high energy species in plasma could tailor the surface composition of catalysts *via* breaking the original chemical bonds on their surface and forming new chemical bonds. Taking advantage of the unique properties of plasma, Liu *et al.* treated BN with N_2 plasma and demonstrated that the N_2 plasma treated BN exhibited a propane conversion of 26.0% and a total selectivity towards propylene and ethene of 89.4% at 520 °C in O_2-ODHP.[122] Characterization revealed that the treatment by N_2 plasma broke the chemical bonds in BN and selectively eliminated the N atoms on the surface of BN, leading to the generation of more N-defects located at three boron centers. The three-boron center N-defects could further be evolved into BO_x, which served as the active sites for O_2-ODHP.

In order to study the active sites of the BN catalyst in O_2-ODHP, understand the reaction pathway of O_2-ODHP on the BN catalyst at the molecular/atomic level, and lay a theoretical foundation for the design of an efficient BN catalyst, researchers analyzed the structure of the BN catalyst and explored the mechanism of BN in O_2-ODHP. For example, combining kinetic analysis and theoretical calculations, Hermans *et al.* proposed that the oxygen terminal site on the hexagonal BN armchair

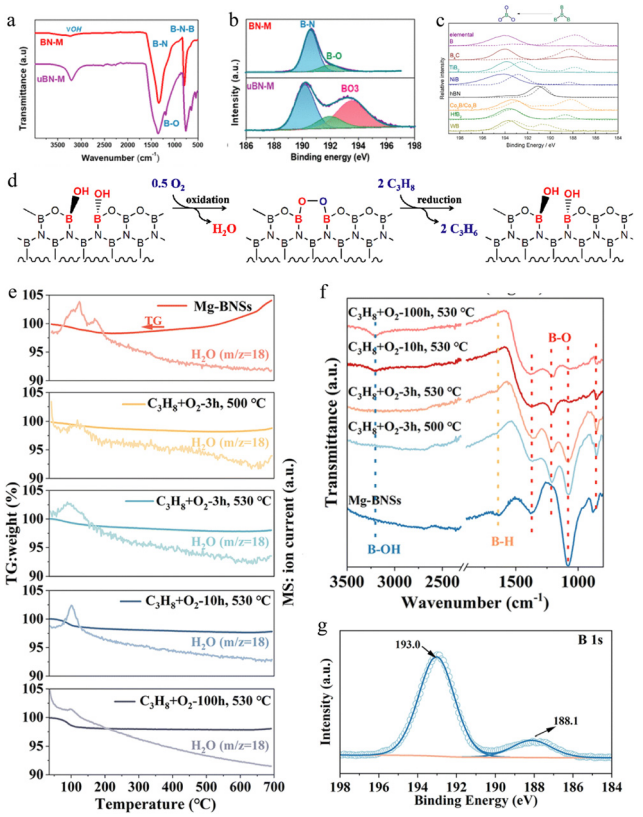

Fig. 6 (a) FTIR and (b) B 1s high-resolution spectra of BN-M and uBN-M.[124] Copyright 2021 American Chemical Society. (c) The XPS B 1s feature of fresh (dotted) and spent (solid) B-containing catalysts.[123] Copyright 2016 Science. (d) The proposed redox reaction cycle in the oxidative dehydrogenation of propane over boron nitride.[126] Copyright 2018 Elsevier. (e) TG-MS analysis of Mg-BNSs and their spent forms under an O_2-rich atmosphere (20% O_2 + 80% N_2). (f) FT-IR spectra of Mg-BNSs and the spent Mg-BNSs activated in the reaction atmosphere at different temperatures and durations. (g) B 1s XPS spectrum of Mg-BNSs tested for 100 h over ODHP.[18] Copyright 2023 Royal Society of Chemistry.

edge >B–O–O–B< was the catalytic active site, >B–O–O–B< activated the second hydrogen atom of propane, while breaking the O–O bond to form boron hydroxyl groups and nitrogen oxygen radicals.[118] The authors further analyzed the surface elements of the catalyst using XPS and found that in O_2-ODHP, BO_x species gradually formed on the BN surface and tended to stabilize, suggesting that the BO_x species were the active site.[125] Hermans *et al.* used ^1H–^{11}B coupling nuclear magnetic resonance and X-ray absorption spectroscopy to investigate the structural changes of the BN catalyst before and after the reaction, determining that the active site of the BN catalyst was a three coordinated boron site ($B(OH)_xO_{3-x}$) with a variable number of hydroxyl groups and bridging oxidation groups, rather than the oxygen terminal site on the armchair edge >B–O–O–B<.[123] Lu *et al.* found that BN exhibited excellent activity and olefin selectivity only after undergoing an activity induction period in O_2-ODHP. XPS and *in situ* XRD characterization confirmed that surface BO_x species gradually formed and tended to stabilize during the oxidative dehydrogenation reaction (Fig. 6c), showing a consistent trend with catalyst activity, confirming that BO_x species were active sites as proposed by Hermans *et al.*[126,127] However, further combining kinetic analysis, Lu *et al.* claimed that the B–OH dynamically generated on the catalyst surface was the active site of the catalyst (Fig. 6d).

Besides the above-mentioned several species, boron atoms at the defective sites,[128] boron-atom-terminated zigzag,[129] and N_2O or NO_x-type sites[130] have also been reported as active sites on BN in O_2-ODHP. Therefore, currently, there is still controversy over the active site of BN in O_2-ODHP. Researchers need to devote more effects to make clear which one is the intrinsic active site for O_2-ODHP over a specific catalytic system.

6.2. Other B-containing catalysts

In addition to BN, some other B-containing catalysts, such as exfoliated boron nanosheets,[18] boron carbonitride,[131] boron phosphate (BPO_4),[132] boron carbide,[133] boron phosphide and silicon boride,[134] and boron-containing metal–organic frameworks,[7] have also been developed for catalytic O_2-ODHP. Here we take the application of exfoliated boron nanosheets in O_2-ODHP as an example for illustration. Zhang *et al.* exfoliated layered MgB_2 with hydrochloric acid to synthesize exfoliated boron nanosheets (Mg-BNSs) for O_2-ODHP.[18] It was revealed that the exfoliated boron nanosheet afforded a propylene and ethylene selectivity of 63.5% and 18.4%, respectively, at a propane conversion of 40.0% at 530 °C, with the olefin productivity much superior to that of the commercial h-BN and other reported boron-based catalysts. In addition, the exfoliated boron nanosheet maintained excellent stability in O_2-ODHP at 530 °C for 100 hours. The dynamic evolution of their structure and surface functional groups under reaction conditions have been investigated for clarifying the origin of the excellent performance of Mg-BNSs. Thermogravimetric analysis with mass spectroscopy (TG-MS) showed an obvious weight loss of fresh Mg-BNSs under 200 °C (Fig. 6e). However, the mass increase started at 400 °C, suggesting the continuous oxidation of Mg-BNSs under an oxygen-rich atmosphere. In contrast, if the sample was activated at 500 or 530 °C for over 3 h under the reaction atmosphere, almost no mass decline could be monitored. Thus, the oxidized form was the main factor for the high activity, because it could avoid the coke formation. In addition, the FTIR spectra observed the B–OH and B–O bonds at 1367, 1200, and 860 cm^{-1} (Fig. 6f), which have been reported as the real active sites for O_2-ODHP. The spent Mg-BNSs exposed more oxygen atoms at the surface and exhibited a more pronounced peak for B–O in the B 1s XPS spectrum (Fig. 6g). These results indicated that the activity of Mg-BNSs was from a large number of generated B–O active sites. This work displayed the huge potential of B-based catalysts for O_2-ODHP under harsh reaction conditions. Considering the low price of MgB_2, B-based catalysts could be a better choice for the O_2-ODHP reaction.

6.3. C-Based catalysts

In 1987, Schraut *et al.* unexpectedly discovered that carbon deposition could induce the oxidative dehydrogenation reaction of ethylbenzene, which opened up the research on C-based

catalysts in the field of oxidative dehydrogenation of low-carbon alkanes. Nanocarbon is a promising catalyst for O_2-ODHP due to its abundant reactive oxygen species, resistance to carbon deposition, and unique electronic and structural properties. However, the unsatisfactory propylene selectivity and low durability under high temperature or O_2-rich conditions restrict the development of carbon-based catalysts. Fortunately, more and more strategies have been proposed to overcome these disadvantages and improve the catalytic performance of nanocarbon catalysts toward O_2-ODHP implementation.

Different C-based catalysts with 2D or 3D morphologies, including carbon nanotubes (CNTs),[135] carbon nanofibers,[136] nanodiamonds,[137] *etc.*, have been applied in O_2-ODHP. Generally, these C-based catalysts have been modified with the aim of improving their catalytic performance. For instance, Frank *et al.* modified carbon nanotubes with boron or phosphorus and investigated the effects of heteroatoms in O_2-ODHP.[135] It was revealed that the introduction of both boron and phosphorus increased the apparent activation energy of the catalyst and the reaction order of oxygen while affecting little the reaction order of propane. It indicated that boron or phosphorus can inhibit the formation of electrophilic oxygen-active sites, where phosphorus was more effective. The inhibited formation of electrophilic oxygen active sites prohibited the overoxidation of propane and propylene and thus improved the selectivity towards propylene. As a result, the modification of carbon nanotubes with phosphorus enhanced the thermal stability of carbon nanotubes, achieving a propane conversion of 7.0% at a selectivity of propylene of about 50.0% (Fig. 7a and b). Chen *et al.* doped nitrogen into carbon nanotubes to regulate the types of functional groups on their surface, and investigated their performance in O_2-ODHP.[138] It was demonstrated that nitrogen doping helped to increase the surface charge density of carbon nanotubes, leading to a strengthened repulsive force between carbon nanotubes and propylene. It was beneficial for reducing the adsorption of propylene on the catalyst, avoiding the overoxidation of propylene, and consequently improving the selectivity towards propylene (Fig. 7c and d).

Another strategy was reported by Qi *et al.*, who utilized heteroatom co-doped polymers (PZS) and oxidized CNTs, achieving 63% propylene selectivity at 14.3% propane

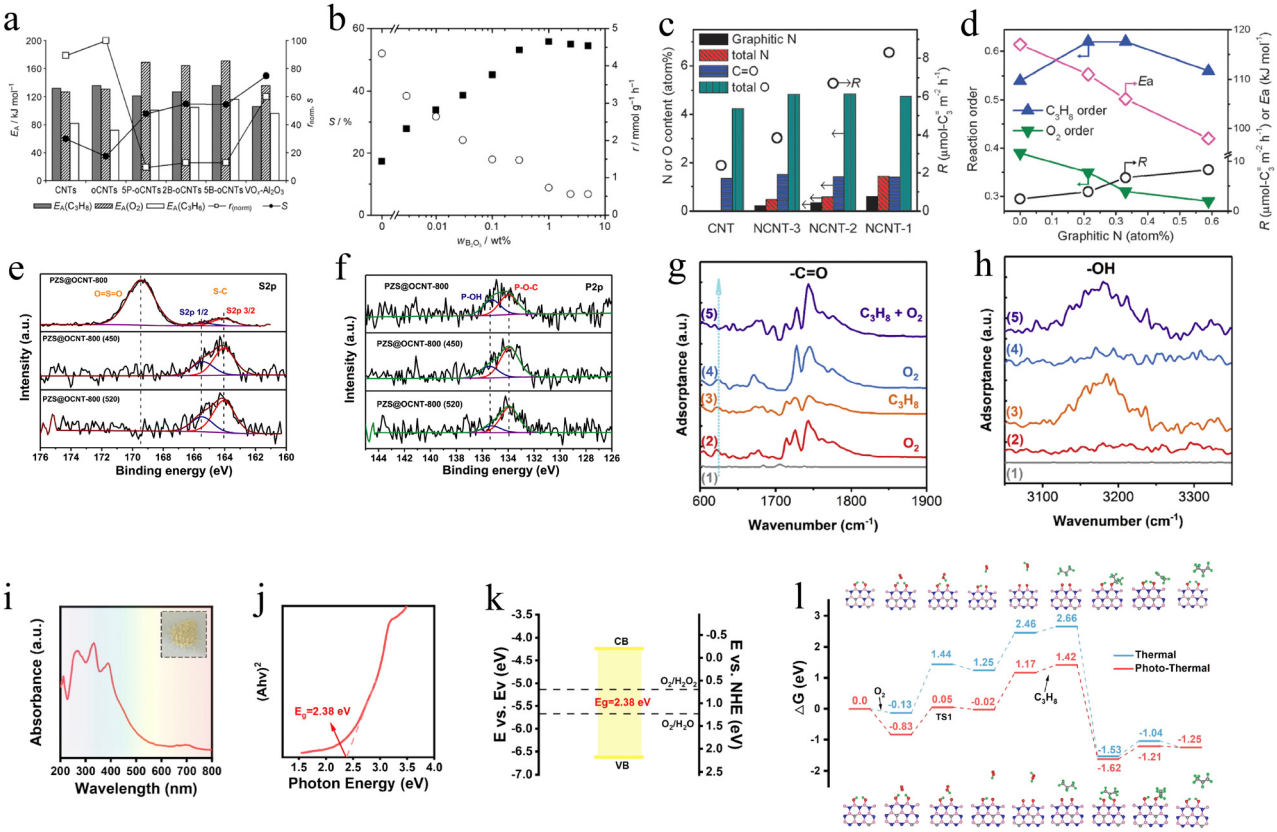

Fig. 7 (a) Catalytic performance of carbon nanotube catalysts in ODHP, with VO_x–Al_2O_3 as a reference. (b) Propylene selectivity at 5% propane conversion (■) and reaction rate r (○) as a function of B_2O_3 loading ($W_{B_2O_3}$). Reproduced with permission from ref. 135. Copyright 2009 Wiley. (c) Structural parameters and C_3H_6 formation rates of spent catalysts. (d) Reaction orders, C_3H_6 formation rates, and activation energy as a function of graphitic N content. Reproduced with permission.[138] Copyright 2013 Royal Society of Chemistry. Deconvolution of (e) S 2p and (f) P 2p XPS signals for PZS@OCNT-800 before and after ODHP reactions (450 °C and 520 °C).[139] Copyright 2022 Elsevier. (g) and (h) *In situ* DRIFT difference spectra at steady state after switching various reaction atmospheres at 500 °C.[140] Copyright 2020 Elsevier. (i) UV-DRS of SS-BCNNSs. (j) Dependence of $(Ahv)^2$ on the photon energy. (k) Schematic band structure of SS-BCNNSs. (l) DFT calculated energy profile for ODHP under thermal and photo-thermal conditions.[141] Copyright 2023 Elsevier.

conversion.[139] What's more, the poor stability of CNTs has also been improved, realizing more than 20 h O_2-ODHP reactions at 520 °C. The kinetic tests conducted at different propane and oxygen partial pressures demonstrated that the as-prepared CNT-based catalysts have excellent resistance to oxidation and carbon deposition, which is the reason for the enhanced stability. The XPS spectra could detect the P–O and S–C species on the catalyst surface, which contributed to the improvement of propylene selectivity and oxidation resistance (Fig. 7e and f).

In spite of the fact that C-based catalysts exhibited a certain activity in O_2-ODHP, due to the complex types of functional groups on the surface of C-based materials (such as hydroxyl group, carbonyl group, anhydride group, lactone group, *etc.*), the qualitative and quantitative determination of effective functional groups has always been a research difficulty in the field of O_2-ODHP.[142] In addition, the complex variety of functional groups on the surface of C-based catalysts makes the reaction more complex. The oxidative dehydrogenation process as well as the overoxidation of propane and propylene might occur. The multiple parallel reaction pathways and diverse intermediates make it challenging to use C-based catalysts in O_2-ODHP.[143]

A series of carbon nitride (CN) polymers provided more opportunities for further developing C-based catalysts with high selectivity in the O_2-ODHP field. For instance, graphitic CN has been reported as an O_2-ODHP catalyst achieving a propane conversion of 12.8% and a selectivity of 74.7% for the desired propylene product.[140] *In situ* DRIFTS characterization showed the orderly formation of –C═O and –OH species (Fig. 7g and h). Accordingly, the authors speculated the reaction pathway. Specifically, the C═O abstracted H atoms from propane to generate propylene and formed C–OH. Subsequently, the following O_2 treatment extracted H atoms from C–OH species and re-generated C═O groups. The switch between C═O and C–OH groups under the reactant atmosphere drove the O_2-ODHP process while avoiding the direct interaction between C_3H_8 and O_2. Theoretically, DFT calculations predicted a reasonable O_2-ODHP reaction pathway, during which two adjacent C═O groups on the edge of CN can activate two C–H bonds of propane simultaneously, thus avoiding the generation of free C_3H_7* radicals and leading to the high selectivity of light olefins.

Due to the high light absorption ability of C-based materials, photothermal catalytic technology has emerged as a novel strategy to trigger O_2-ODHP reaction under mild conditions. Compared to traditional reaction conditions, the lower reaction temperature during photothermal catalysis benefits the control of propylene selectivity and catalyst stability. One recent example is based on a semiconducting boron CN (BCN) catalyst, which integrated photocatalysis with thermal catalysis.[141] The fundamental theory is the cooperation between electrically conductive properties from the graphene phase and insulation from boron nitride (h-BN). Thus, the BCN alloy could possess both excellent catalytic performance of h-BN towards O_2-ODHP and the semiconductor behavior of graphene. Ultraviolet-visible diffuse reflectance spectroscopy (UV-DRS) showed the effective visible light response of BCN with a 500 nm absorption edge (Fig. 7i). And the Tauc plot clarified that BCN was a direct band gap material, which had a band gap of 2.83 eV (Fig. 7j). According to ultraviolet photoelectron spectroscopy (UPS) measurements, the authors determined the energy band structure of BCN with 3.92 eV *vs.* evac conduction band and 6.62 eV *vs.* evac valence band, indicating the photocatalytic ability for activating O_2 (Fig. 7k). At 480 °C, the propane conversion increased from 11.1% to 21.2% *via* light irradiation, resulting in an increase in the overall yield of olefin from 10.4% to 19.6% and higher propylene selectivity. DFT results clearly showed the advantage of photothermal catalysis in terms of the energy barrier and the rate-determining step (the dehydrogenation of B-OH groups to form BO·) in the BCN catalytic system (Fig. 7l). Indeed, this work confirmed the great potential of integrating photocatalysis with conventional thermal catalysis *via* semiconductor catalysts to enhance propane conversion and propylene selectivity during the O_2-ODHP reaction. The photothermal method will play a key role in achieving carbon neutrality.

7. Summary and outlook

To date, a wide variety of catalysts have been developed for O_2-ODHP, such as transition metal oxide catalysts, transition metal-based catalysts, rare earth metal oxide catalysts, and non-metallic catalysts. Some typical examples of the catalysts are displayed in Table 1. The current challenges and coping strategies are summarized below.

(1) Despite the variety of catalysts developed for O_2-ODHP, to the best of our knowledge, the highest yield towards propylene was achieved over the NiO–CeO_2 catalyst, up to 55.0%, with a propane conversion of 69.0% and a selectivity towards propylene of 80.0%. Apparently, their performances are still far away from industrialization. In addition, for most of the catalytic systems, it is still challenging to realize a high propane conversion rate and high selectivity towards propylene simultaneously. Therefore, in the future, it is demanded to develop a novel catalyst, which can achieve high selectivity towards propylene at high propane conversion rates.[144,145]

(2) Even though characterization and theoretical calculations have been conducted over some of the catalytic systems, the intrinsic mechanism remains unclear. As is known, the catalytic reaction mechanism plays an important role in guiding the development of more advanced and efficient catalysts. Therefore, in the future, more studies should be focused on the investigation of the reaction system, using *in situ*/*operando* characterization techniques as well as theoretical simulations, to unravel the intrinsic active site and reaction pathways of the O_2-ODHP process.

(3) Considering the two facts that (i) propane as the reactant has to be extracted from other raw materials like shale gas and (ii) propylene is important for downstream chemical reactions to get high value-added products, the coupling between O_2-ODHP and other catalytic reactions should be paid more

Table 1 Some typical examples of catalysts developed for ODHP

Catalyst	Reaction condition	Performance	Ref.
V_2O_5/SiO_2	Reactor type: conventional continuous flow quartz microreactor Reactant ratio: $C_3H_8:O_2:N_2:He = 2:1:1:6$ Reactant feed: GHSV = 1700 h^{-1} Reaction temperature: 450 °C Reaction pressure: 1 atm	Selectivity towards propylene is 72.0%	16
$ZrMo_2O_8/ZrO_2$	Reactor type: packed-bed tubular quartz reactor Reactants: propane and oxygen at 14.03 and 1.74 kPa Reaction temperature: 500 °C	Selectivity towards propylene is 80.0%	23
Ti–Ni–O	Reactant ratio: $C_3H_8:O_2:N_2 = 1.1:1:4$ Reactant feed: 9000 mL h^{-1} g^{-1} Reaction temperature: 300 °C	Propane conversion is about 28.4%, selectivity to propylene is 42.5% and propylene yield is 12.1%	36
$MoVO_x$	Reactor type: fixed bed reactor Reactant ratio: $C_3H_8:O_2:N_2 = 6:3:91$ Reaction temperature: 350 °C	Propane conversion is about 2.7%, selectivity to propylene is 100% and propylene yield is 2.7%	45
Pt–Ce/γ-Al_2O_3	Reactor type: freestanding anaerobic-anoxic-oxic flow reactor setup Reactant ratio: $C_3H_8:H_2:Ar = 1:1:5$ Reaction temperature: 576 °C	Propane conversion is about 37.0% and selectivity to propylene is 96.0%	49
Ni-CA SACs	Reactor type: fixed bed reactor Reactant ratio: $C_3H_8:O_2:N_2 = 2:1:17$ Reactant feed: WHSV = 12 000 L kg_{cat}^{-1} h^{-1} Reaction temperature: 580 °C Reaction pressure: 1 atm	Selectivity to propylene is 47.3% and propylene yield is 14.2%	53
NiO−CeO_2	Reactor type: fixed-bed flow reactor Reactant ratio: $C_3H_8:HCl:O_2 = 9:9:5$ Reactant feed: 48 mL min^{-1} Reaction temperature: 500 °C Reaction pressure: 1 atm	Propane conversion is about 69.0%, selectivity to propylene is 80.0% and propylene yield is 55.0%	57
P-CeO_2	Reactor type: fixed-bed quartz tube down-flow reactor Reactant ratio: C_3H_8 : air = 1 : 2.5 Reactant feed: VHSV = 9000 h^{-1} Reaction temperature: 600 °C	Propane conversion is about 8.7% and selectivity to propylene is 70.1%	59
h-BN	Reactor type: quartz tube reactor Reactants: 0.15 atm O_2 and 0.3 atm C_3H_8 Reaction temperature: 490 °C.	Propane conversion is about 14.0% and selectivity to propylene is 79.0%	65
BNOH	Reactor type: packed-bed quartz microreactor Reactant ratio: $C_3H_8:O_2:He = 1:1.5:3.5$ Reactant feed: 192 mL min^{-1} Reaction temperature: 530 °C	Propane conversion is about 20.6% and selectivity to propylene is 80.2%.	66
BN with a larger specific surface area	Reactor type: fixed-bed reactor Reactant ratio: $C_3H_8:O_2:He = 1:50:49$ Reactant feed: 20 mL min^{-1} Reaction temperature: 525 °C Reaction pressure: 1 atm	Propane conversion is about 50.0% and selectivity to propylene is 70.0%	67
N_2 plasma treated BN	Reactor type: packed-bed quartz reactor Reactant ratio: $C_3H_8:O_2:Ne = 1:1.5:3.5$ Reactant feed: 48 mL min^{-1} Reaction temperature: 520 °C Reaction pressure: atmospheric pressure	Propane conversion is 26.0% and the total selectivity towards propylene and ethene is 89.4%	69
B_4C	Reactor type: quartz reactor tube Reactant ratio: $C_3H_8:O_2:N_2 = 6:3:11$ Reactant feed: $WHSV^{-1}$ = 10.5 kg-cat * s mol^{-1} C_3H_8 Reaction temperature: 500 °C Reaction pressure: 0.30 atm C_3H_8 and 0.15 atm O_2	Propane conversion is about 5.1% and selectivity to propylene is 86.0%	73
Ti_2B	Reactor type: quartz reactor tube Reactant ratio: $C_3H_8:O_2:N_2 = 6:3:11.$ Reactant feed: $WHSV^{-1}$ = 12.5 kg-cat * s mol^{-1} C_3H_8 Reaction temperature: 500 °C Reaction pressure: 0.30 atm C_3H_8 and 0.15 atm O_2	Propane conversion is about 5.2% and selectivity to propylene is 85.3%	73
Exfoliated layered MgB_2	Reactor type: fixed-bed reactor Reactant ratio: $C_3H_8:O_2:N_2 = 1:1:3$ Reactant feed: WHSV = 24 000 mL g^{-1} h^{-1} Reaction temperature: 530 °C Reaction pressure: atmospheric pressure	Propane conversion is about 39.8%, selectivity to propylene is 63.5% and propylene yield is 26.3%	78
N doped CNT	Reactor type: immobilized bed quartz reactor Reactant ratio: $C_3H_8:O_2:$ He = 2 : 1 : 19 Reactant feed: GHSV = 13 L g^{-1} h^{-1} Reaction temperature: 400 °C Reaction pressure: atmospheric pressure	Propane conversion is about 5.0% and selectivity to propylene is 56.5%	82

attention to realize the large-scale industrialization and even achieve the green chemistry and carbon neutral aims. For this aim, a cheaper catalyst should be designed and developed to meet the requirements of continuous and large-scale catalytic reactions. What's more, the reaction vessel for conducting different catalytic processes should also be constructed to promote the advanced catalytic systems involving the combination of the shale gas–propane conversion and O_2-ODHP, and the coupling between O_2-ODHP and reactions converting propylene into value-added products.

Data availability

No primary research results, software or code have been included and no new data were generated or analysed as part of this review.

Conflicts of interest

There are no conflicts to declare.

Acknowledgements

This work received financial support from the Young Talent Plan of Liaoning Province (XLYC2203068), Scientific Research Foundation of Technology Department of Liaoning Province of China (2022-MS-379), and National Natural Science Foundation of China (21902116). Financial support from the program of China Scholarships Council (No. 202206250016) is gratefully acknowledged.

Notes and references

1 W. Wu, W. Guo, W. Xiao and M. Luo, *Chem. Eng. Sci.*, 2011, **66**, 4722–4732.
2 A. K. Sinha, S. Seelan, S. Tsubota and M. Haruta, *Angew. Chem., Int. Ed.*, 2004, **43**, 1546–1548.
3 H. Oikawa, Y. Shibata, K. Inazu, Y. Iwase, K. Murai, S. Hyodo, G. Kobayashi and T. Baba, *Appl. Catal., A*, 2006, **312**, 181–185.
4 L. Schumacher, J. Shen, K. Hofmann and C. Hess, *Catal. Today*, 2024, **426**, 114387.
5 M. L. Sarazen and C. W. Jones, *J. Phys. Chem. C*, 2018, **122**, 28637–28644.
6 X. Fan, D. Liu, X. Sun, X. Yu, D. Li, Y. Yang, H. Liu, J. Diao, Z. Xie, L. Kong, X. Xiao and Z. Zhao, *J. Catal.*, 2020, **389**, 450–460.
7 L. Cao, P. Dai, S. Wen, Y. Jiang, D. Liu, X. Gu, Q. Zhang, Y. Xia, G. Zhong, X. Zhao and J. Xie, *Matter*, 2023, **6**, 4376–4387.
8 A. Al-Douri, D. Sengupta and M. M. El-Halwagi, *J. Nat. Gas Sci. Eng.*, 2017, **45**, 436–455.
9 J. Guo, Y. Lei, H. Liu, Y. Li, D. Li and D. He, *Catal. Sci. Technol.*, 2023, **13**, 4045–4063.
10 Y. Li, Y. Lei, D. Li, A. Liu, Z. Zheng, H. Liu, J. Guo, S. Liu, C. Hao and D. He, *ACS Catal.*, 2023, 10177–10204.
11 Y. Lei, J. Ye, J. García-Antón and H. Liu, *Chin. J. Catal.*, 2023, **53**, 72–101.
12 S. Hu, P. Qiao, X. Yi, Y. Lei, H. Hu, J. Ye and D. Wang, *Angew. Chemie*, 2023, **135**, e202304585.
13 Y. Lei, Z. Jia, H. Hu, L. Liu, J. Ye and D. Wang, *Catalysts*, 2022, **12**, 1323.
14 S. Sokolov, V. Y. Bychkov, M. Stoyanova, U. Rodemerck, U. Bentrup, D. Linke, Y. P. Tyulenin, V. N. Korchak and E. V. Kondratenko, *ChemCatChem*, 2015, **7**, 1691–1700.
15 S. Sokolov, M. Stoyanova, U. Rodemerck, D. Linke and E. V. Kondratenko, *Catal. Sci. Technol.*, 2014, **4**, 1323.
16 B. Hu, W. Kim, T. P. Sulmonetti, M. L. Sarazen, S. Tan, J. So, Y. Liu, R. S. Dixit, S. Nair and C. W. Jones, *ChemCatChem*, 2017, **9**, 3330–3337.
17 A. Siahvashi, D. Chesterfield and A. A. Adesina, *Ind. Eng. Chem. Res.*, 2013, **52**, 4017–4026.
18 D. Zhang, S. Wang, C. Zhang, L. He and W. Sun, *Nanoscale*, 2024, **16**, 1312–1319.
19 S. Vajda, M. J. Pellin, J. P. Greeley, C. L. Marshall, L. A. Curtiss, G. A. Ballentine, J. W. Elam, S. Catillon-Mucherie, P. C. Redfern, F. Mehmood and P. Zapol, *Nat. Mater.*, 2009, **8**, 213–216.
20 F. Cavani, N. Ballarini and A. Cericola, *Catal. Today*, 2007, **127**, 113–131.
21 T. Blasco and J. M. L. Nieto, *Appl. Catal., A*, 1997, **157**, 117–142.
22 R. Grabowski, *Catal. Rev.*, 2006, **48**, 199–268.
23 P. Concepción, J. M. López Nieto and J. Pérez-Pariente, *Catal. Lett.*, 1993, **19**, 333–337.
24 J. M. López Nieto, P. Concepción, A. Dejoz, H. Knözinger, F. Melo and M. I. Vázquez, *J. Catal.*, 2000, **189**, 147–157.
25 S. Chen, X. Chang, G. Sun, T. Zhang, Y. Xu, Y. Wang, C. Pei and J. Gong, *Chem. Soc. Rev.*, 2021, **50**, 3315–3354.
26 Y. Yuan, W. N. Porter and J. G. Chen, *Trends Chem.*, 2023, **5**, 840–852.
27 J. H. Carter, T. Bere, J. R. Pitchers, D. G. Hewes, B. D. Vandegehuchte, C. J. Kiely, S. H. Taylor and G. J. Hutchings, *Green Chem.*, 2021, **23**, 9747–9799.
28 Y. Gambo, S. Adamu, A. A. Abdulrasheed, R. A. Lucky, M. S. Ba-Shammakh and M. M. Hossain, *Appl. Catal., A*, 2021, **609**, 117914.
29 X. Jiang, L. Sharma, V. Fung, S. J. Park, C. W. Jones, B. G. Sumpter, J. Baltrusaitis and Z. Wu, *ACS Catal.*, 2021, **11**, 2182–2234.
30 X. Gao, M. Liu, Y. Huang, W. Xu, X. Zhou and S. Yao, *ACS Catal.*, 2023, **13**, 9667–9687.
31 Z.-P. Hu, D. Yang, Z. Wang and Z.-Y. Yuan, *Chin. J. Catal.*, 2019, **40**, 1233–1254.
32 M. A. Atanga, F. Rezaei, A. Jawad, M. Fitch and A. A. Rownaghi, *Appl. Catal., B*, 2018, **220**, 429–445.
33 E. Gomez, B. Yan, S. Kattel and J. G. Chen, *Nat. Rev. Chem.*, 2019, **3**, 638–649.
34 F. Xing, Y. Nakaya, S. Yasumura, K. Shimizu and S. Furukawa, *Nat. Catal.*, 2022, **5**, 55–65.
35 S. Song, X. Chen, Y. Fo, M. Yang, H. Su, K. Yang, X. Ji, X. Lv, Z. Li, Y. Wei, G. Huang, C. Xu, J. Liu and W. Song, *Chem. Catal.*, 2023, **3**, 100663.
36 E. Gomez, Z. Xie and J. G. Chen, *AIChE J.*, 2019, **65**, e16670.
37 E. Gomez, S. Kattel, B. Yan, S. Yao, P. Liu and J. G. Chen, *Nat. Commun.*, 2018, **9**, 1398.
38 L. M. Neal, S. Yusuf, J. A. Sofranko and F. Li, *Energy Technol.*, 2016, **4**, 1200–1208.
39 T. Wu, Q. Yu, K. Wang and M. van Sint Annaland, *Catalysts*, 2021, **11**, 119.
40 S. Yusuf, V. Haribal, D. Jackson, L. Neal and F. Li, *Appl. Catal., B*, 2019, **257**, 117885.
41 J. Baek, H. J. Yun, D. Yun, Y. Choi and J. Yi, *ACS Catal.*, 2012, **2**, 1893–1903.
42 S. Wang and Z. H. Zhu, *Energy Fuels*, 2004, **18**, 1126–1139.
43 T. Wu, Q. Yu and Q. Qin, *Pet. Sci. Technol.*, 2018, **36**, 266–272.
44 E. A. de Graaf, G. Rothenberg, P. J. Kooyman, A. Andreini and A. Bliek, *Appl. Catal., A*, 2005, **278**, 187–194.
45 N. Ballarini, F. Cavani, A. Cericola, C. Cortelli, M. Ferrari, F. Trifirò, G. Capannelli, A. Comite, R. Catani and U. Cornaro, *Catal. Today*, 2004, **91–92**, 99–104.
46 X. Wang, C. Pei, Z.-J. Zhao, S. Chen, X. Li, J. Sun, H. Song, G. Sun, W. Wang, X. Chang, X. Zhang and J. Gong, *Nat. Commun.*, 2023, **14**, 2039.
47 T. Wu, Q. Yu, L. Hou, W. Duan, K. Wang and Q. Qin, *J. Therm. Anal. Calorim.*, 2020, **140**, 1837–1843.
48 T. Wu, Q. Yu, I. Roghair, K. Wang and M. van Sint Annaland, *Chem. Eng. Process. - Process Intensif.*, 2020, **157**, 108137.
49 A. Hameed, M. A. Gondal and Z. H. Yamani, *Catal. Commun.*, 2004, **5**, 715–719.
50 T. Otroshchenko, G. Jiang, V. A. Kondratenko, U. Rodemerck and E. V. Kondratenko, *Chem. Soc. Rev.*, 2021, **50**, 473–527.

51 A. Khodakov, B. Olthof, A. T. Bell and E. Iglesia, *J. Catal.*, 1999, **181**, 205–216.
52 M. Puglisi, F. Arena, F. Frusteri, V. Sokolovskii and A. Parmaliana, *Catal. Lett.*, 1996, **41**, 41–43.
53 Y. Liu, Y. Cao, N. Yi, W. Feng, W. Dai, S. Yan, H. He and K. Fan, *J. Catal.*, 2004, **224**, 417–428.
54 Y. Liu, W. Feng, T. Li, H. He, W. Dai, W. Huang, Y. Cao and K. Fan, *J. Catal.*, 2006, **239**, 125–136.
55 Z. Han, X. Xue, J. Wu, W. Lang and Y. Guo, *Chin. J. Catal.*, 2018, **39**, 1099–1109.
56 M. J. Ndolomingo, N. Bingwa and R. Meijboom, *J. Mater. Sci.*, 2020, **55**, 6195–6241.
57 H. H. Kung, *Advances in Catalysis*, 1994, pp. 1–38.
58 J. T. Grant, C. A. Carrero, A. M. Love, R. Verel and I. Hermans, *ACS Catal.*, 2015, **5**, 5787–5793.
59 J. Schönherr, K. Eckl and H. Gruler, *Planta*, 1979, **147**, 21–26.
60 K. Chen, S. Xie, A. T. Bell and E. Iglesia, *J. Catal.*, 2001, **198**, 232–242.
61 A. Parmaliana, V. Sokolovskii, D. Miceli and N. Giordano, *Appl. Catal., A*, 1996, **135**, L1–L5.
62 A. Corma, J. M. L. Nieto and N. Paredes, *J. Catal.*, 1993, **144**, 425–438.
63 X. T. Gao, P. Ruiz, Q. Xin, X. X. Guo and B. Delmon, *J. Catal.*, 1994, **148**, 56–67.
64 F. Ying, J. Li, C. Huang, W. Weng and H. Wan, *Catal. Lett.*, 2007, **115**, 137–142.
65 K. Chen, S. Xie, E. Iglesia and A. T. Bell, *J. Catal.*, 2000, **189**, 421–430.
66 K. Chen, S. Xie, A. T. Bell and E. Iglesia, *J. Catal.*, 2000, **195**, 244–252.
67 G. Lin, Y. Su, X. Duan and K. Xie, *Angew. Chem., Int. Ed.*, 2021, **60**, 9311–9315.
68 O. Lezla, E. Bordes, P. Courtine and G. Hecquet, *J. Catal.*, 1997, **170**, 346–356.
69 T. E. Davies, T. García, B. Solsona and S. H. Taylor, *Chem. Commun.*, 2006, 3417–3419.
70 S. Song, J. Li, Z. Wu, P. Zhang, Y. Sun, W. Song, Z. Li and J. Liu, *AIChE J.*, 2022, **68**, e17451.
71 Z. Li, A. W. Peters, V. Bernales, M. A. Ortuño, N. M. Schweitzer, M. R. DeStefano, L. C. Gallington, A. E. Platero-Prats, K. W. Chapman, C. J. Cramer, L. Gagliardi, J. T. Hupp and O. K. Farha, *ACS Cent. Sci.*, 2017, **3**, 31–38.
72 Z. Li, A. W. Peters, A. E. Platero-Prats, J. Liu, C.-W. Kung, H. Noh, M. R. DeStefano, N. M. Schweitzer, K. W. Chapman, J. T. Hupp and O. K. Farha, *J. Am. Chem. Soc.*, 2017, **139**, 15251–15258.
73 M.-X. Huang, X. Wu, X.-D. Yi, G.-B. Han, W.-S. Xia and H.-L. Wan, *RSC Adv.*, 2017, **7**, 14846–14856.
74 A. W. Peters, K. Otake, A. E. Platero-Prats, Z. Li, M. R. DeStefano, K. W. Chapman, O. K. Farha and J. T. Hupp, *ACS Appl. Mater. Interfaces*, 2018, **10**, 15073–15078.
75 Y. Liu, R. Che, G. Chen, J. Fan, Z. Sun, Z. Wu, M. Wang, B. Li, J. Wei, Y. Wei, G. Wang, G. Guan, A. A. Elzatahry, A. A. Bagabas, A. M. Al-Enizi, Y. Deng, H. Peng and D. Zhao, *Sci. Adv.*, 2015, **1**, e1500166.
76 J.-H. Li, C.-C. Wang, C.-J. Huang, Y.-F. Sun, W.-Z. Weng and H.-L. Wan, *Appl. Catal., A*, 2010, **382**, 99–105.
77 Z. Teng, G. Zheng, Y. Dou, W. Li, C. Mou, X. Zhang, A. M. Asiri and D. Zhao, *Angew. Chem., Int. Ed.*, 2012, **51**, 2173–2177.
78 D. Li, H. Zhou and I. Honma, *Nat. Mater.*, 2004, **3**, 65–72.
79 X. Fan, D. Liu, Z. Zhao, J. Li and J. Liu, *Catal. Today*, 2020, **339**, 67–78.
80 Y. Wu, Y. He, T. Chen, W. Weng and H. Wan, *Appl. Surf. Sci.*, 2006, **252**, 5220–5226.
81 J. Li, C. Wang, C. Huang, W. Weng and H. Wan, *Catal. Lett.*, 2010, **137**, 81–87.
82 Q. Xie, H. Zhang, J. Kang, J. Cheng, Q. Zhang and Y. Wang, *ACS Catal.*, 2018, **8**, 4902–4916.
83 Y. He, Y. Wu, T. Chen, W. Weng and H. Wan, *Catal. Commun.*, 2006, **7**, 268–271.
84 E. Heracleous and A. A. Lemonidou, *J. Catal.*, 2010, **270**, 67–75.
85 W. Cai-Cai, L. Jian-Hui, S. Yi-Fei, Z. Xiao-Quan, H. Chuan-Jing, W. Wei-Zheng and W. Hui-Lin, *Acta Phys.-Chim. Sin.*, 2011, **27**, 2421–2426.
86 A. P. Pushkar and J. J. Varghese, *J. Catal.*, 2022, **413**, 681–691.
87 B. Farin, P. Eloy, C. Poleunis, M. Devillers and E. M. Gaigneaux, *Catal. Sci. Technol.*, 2016, **6**, 6046–6056.
88 L. Huai-Qian, S. Lei, H. Chong, W. Wei-Zheng, H. Chuan-Jing and W. Hui-Lin, *Acta Phys.-Chim. Sin.*, 2012, **28**, 2697–2704.
89 P. Boizumault-Moriceau, *Appl. Catal., A*, 2003, **245**, 55–67.
90 H. Alasiri, S. Ahmed, F. Rahman, A. Al-Amer and U. B. Majeed, *Can. J. Chem. Eng.*, 2019, **97**, 2340–2346.
91 K. Shimoda, S. Ishikawa, K. Matsumoto, M. Miyasawa, M. Takebe, R. Matsumoto, S. Lee and W. Ueda, *ChemCatChem*, 2021, **13**, 3132–3139.
92 A. Massó Ramírez, F. Ivars-Barceló and J. M. López Nieto, *Catal. Today*, 2020, **356**, 322–329.
93 L. Schumacher, J. Pfeiffer, J. Shen, T. Gutmann, H. Breitzke, G. Buntkowsky, K. Hofmann and C. Hess, *ACS Catal.*, 2023, **13**, 8139–8160.
94 A. Bielaski, *J. Catal.*, 1972, **25**, 398–406.
95 X. Zhang, J. Liu, Y. Jing and Y. Xie, *Appl. Catal., A*, 2003, **240**, 143–150.
96 Y. Schuurman, V. Ducarme, T. Chen, W. Li, C. Mirodatos and G. A. Martin, *Appl. Catal., A*, 1997, **163**, 227–235.
97 Q. Zhang, C. Cao, T. Xu, M. Sun, J. Zhang, Y. Wang and H. Wan, *Chem. Commun.*, 2009, 2376.
98 E. Heracleous and A. Lemonidou, *J. Catal.*, 2006, **237**, 162–174.
99 E. Cartuyvels, G. Absillis and T. N. Parac-Vogt, *Chem. Commun.*, 2008, 85–87.
100 A. Proust, R. Thouvenot and P. Gouzerh, *Chem. Commun.*, 2008, 1837.
101 A. Beretta, L. Piovesan and P. Forzatti, *J. Catal.*, 1999, **184**, 455–468.
102 X. Gao, L. Zhu, F. Yang, L. Zhang, W. Xu, X. Zhou, Y. Huang, H. Song, L. Lin, X. Wen, D. Ma and S. Yao, *Nat. Commun.*, 2023, **14**, 1478.
103 M. B. Gawande, K. Ariga and Y. Yamauchi, *Small*, 2021, **17**, 2101584.
104 J. Li, M. F. Stephanopoulos and Y. Xia, *Chem. Rev.*, 2020, **120**, 11699–11702.
105 X. Cui, W. Li, P. Ryabchuk, K. Junge and M. Beller, *Nat. Catal.*, 2018, **1**, 385–397.
106 Y. Xing, L. Kang, J. Ma, Q. Jiang, Y. Su, S. Zhang, X. Xu, L. Li, A. Wang, Z.-P. Liu, S. Ma, X. Y. Liu and T. Zhang, *Chin. J. Catal.*, 2023, **48**, 164–174.
107 Q. Zhang, X. Jiang, Y. Li, Y. Tan, Q. Jiang, X. Liu and B. Qiao, *Chin. J. Chem.*, 2024, **42**, 370–376.
108 R. Peng, S. Li, X. Sun, Q. Ren, L. Chen, M. Fu, J. Wu and D. Ye, *Appl. Catal., B*, 2018, **220**, 462–470.
109 Z. Hu, X. Liu, D. Meng, Y. Guo, Y. Guo and G. Lu, *ACS Catal.*, 2016, **6**, 2265–2279.
110 J. Liu, M. Hao, C. Chen, K. Du, Q. Zhou, S. Zou, L. Xiao and J. Fan, *Appl. Surf. Sci.*, 2020, **528**, 147025.
111 H. L. Wan, X. P. Zhou, W. Z. Weng, R. Q. Long, Z. S. Chao, W. De Zhang, M. S. Chen, J. Z. Luo and S. Q. Zhou, *Catal. Today*, 1999, **51**, 161–175.
112 I. Trotuș, C. M. Teodorescu, V. I. Pârvulescu and I. Marcu, *ChemCatChem*, 2013, **5**, 757–765.
113 J. M. Venegas, W. P. McDermott and I. Hermans, *Acc. Chem. Res.*, 2018, **51**, 2556–2564.
114 C. Xu, C. Ge, D. Sun, Y. Fan and X.-B. Wang, *Nanotechnology*, 2022, **33**, 432003.
115 X. Jiang, K. Zhang, M. J. Forte, S. Cao, B. S. Hanna and Z. Wu, *Catal. Rev.*, 2022, 1–80.
116 H. Chen, D. Jiang, Z. Yang and S. Dai, *Acc. Chem. Res.*, 2023, **56**, 52–65.
117 Z. Fu, D.-Z. Li, L.-D. Zhou, Y.-M. Li, J.-W. Guo, Y.-Q. Li, H.-M. Liu and Q.-J. Zhang, *Pet. Sci.*, 2023, **20**, 2488–2498.
118 J. T. Grant, C. A. Carrero, F. Goeltl, J. Venegas, P. Mueller, S. P. Burt, S. E. Specht, W. P. McDermott, A. Chieregato and I. Hermans, *Science*, 2016, **354**, 1570–1573.
119 L. Shi, D. Wang, W. Song, D. Shao, W. Zhang and A. Lu, *ChemCatChem*, 2017, **9**, 1788–1793.
120 P. Chaturbedy, M. Ahamed and M. Eswaramoorthy, *ACS Omega*, 2018, **3**, 369–374.
121 G. Wang, X. Zhang, Y. Yan, X. Huang and Z. Xie, *Appl. Catal., A*, 2021, **628**, 118402.
122 Z. Liu, B. Yan, S. Meng, R. Liu, W. Lu, J. Sheng, Y. Yi and A. Lu, *Angew. Chem., Int. Ed.*, 2021, **60**, 19691–19695.

123 A. M. Love, B. Thomas, S. E. Specht, M. P. Hanrahan, J. M. Venegas, S. P. Burt, J. T. Grant, M. C. Cendejas, W. P. McDermott, A. J. Rossini and I. Hermans, *J. Am. Chem. Soc.*, 2019, **141**, 182–190.
124 G. Wang, Y. Yan, X. Zhang, X. Gao and Z. Xie, *Ind. Eng. Chem. Res.*, 2021, **60**, 17949–17958.
125 J. T. Grant, W. P. McDermott, J. M. Venegas, S. P. Burt, J. Micka, S. P. Phivilay, C. A. Carrero and I. Hermans, *ChemCatChem*, 2017, **9**, 3623–3626.
126 L. Shi, D. Wang and A. Lu, *Chin. J. Catal.*, 2018, **39**, 908–913.
127 L. Shi, Y. Wang, B. Yan, W. Song, D. Shao and A.-H. Lu, *Chem. Commun.*, 2018, **54**, 10936–10946.
128 D. Creaser, B. Andersson, R. R. Hudgins and P. L. Silveston, *Chem. Eng. Sci.*, 1999, **54**, 4365–4370.
129 H. Li, J. Zhang, P. Wu, S. Xun, W. Jiang, M. Zhang, W. Zhu and H. Li, *J. Phys. Chem. C*, 2019, **123**, 2256–2266.
130 B. Rajbanshi, S. Saha, C. Fricke, S. C. Ammal and A. Heyden, *Catal. Sci. Technol.*, 2020, **10**, 5181–5195.
131 G. Wang, S. Chen, Q. Duan, F. Wei, S. Lin and Z. Xie, *Angew. Chem., Int. Ed.*, 2023, **62**, e202307470.
132 Q. Zhou, Z. Liu, L. Zhu, W. Lu, L. He and D. Wang, *J. Phys. Chem. C*, 2023, **127**, 12942–12952.
133 L. Zhu, Z. Liu, Q. Zhou, W.-D. Lu and D. Wang, *J. Phys. Chem. C*, 2023, **127**, 6280–6293.
134 F. Wu, Z. Liu, J. Sheng, L. Zhu, W.-D. Lu, B. Qiu, D. Wang and A.-H. Lu, *J. Catal.*, 2023, **424**, 121–129.
135 B. Frank, J. Zhang, R. Blume, R. Schlögl and D. S. Su, *Angew. Chem., Int. Ed.*, 2009, **48**, 6913–6917.
136 Z. Sui, J. Zhou, Y. Dai and W. Yuan, *Catal. Today*, 2005, **106**, 90–94.
137 X. Sun, Y. Ding, B. Zhang, R. Huang and D. S. Su, *Chem. Commun.*, 2015, **51**, 9145–9148.
138 C. Chen, J. Zhang, B. Zhang, C. Yu, F. Peng and D. Su, *Chem. Commun.*, 2013, **49**, 8151.
139 T. Cao, X. Dai, W. Liu, Y. Fu and W. Qi, *Carbon N. Y.*, 2022, **189**, 199–209.
140 L. Cao, P. Dai, L. Zhu, L. Yan, R. Chen, D. Liu, X. Gu, L. Li, Q. Xue and X. Zhao, *Appl. Catal., B*, 2020, **262**, 118277.
141 D. Yang, D. Liu, Y. Li, H. Gan, P. Xu, Y. Tian, Z. Li, T. Xing, X. Gu, L. Li, X. Wang, L. Wei, P. Dai and M. Wu, *Appl. Surf. Sci.*, 2023, **639**, 158258.
142 X. Sun, P. Han, B. Li, S. Mao, T. Liu, S. Ali, Z. Lian and D. Su, *Chem. Commun.*, 2018, **54**, 864–875.
143 W. Qi and D. Su, *ACS Catal.*, 2014, **4**, 3212–3218.
144 C. Li, H. Zhang, W. Liu, L. Sheng, M.-J. Cheng, B. Xu, G. Luo and Q. Lu, *Nat. Commun.*, 2024, **15**, 884.
145 K. Zhang, S. Sun and K. Huang, *Chem. Eng. J.*, 2024, **481**, 148395.

